Master's Thesis

Master's degree in Energy Engineering

Study of the Motions and Nacelle Accelerations of the Windcrete Floating Offshore Wind Turbine According to the IEC 64100-3 Procedure

José Manuel Vázquez D'andrea

Supervisors:
Climent Molins
Pau Trubat

April 2020

Escola Tècnica Superior
d'Enginyeria Industrial de Barcelona

Abstract

Floating offshore wind technology is yet to establish a share in the renewable energy market, so far just a few commercial projects exist and many new concepts are being developed and tested. During this stage, simulation soft-wares like FAST are specially useful as they accelerate the development phase of the project, allowing the developers to understand the behaviour of their concepts under different conditions before constructing and testing prototypes. In this work the motions and nacelle accelerations of the Windcrete concept will be studied using FAST and the metocean data of two sites.

Contents

List of Figures

List of Tables

Chapter 1

Introduction

The fast development of the renewable energy sector is now a crucial objective for most of the nations in the world, with this interest, many new technologies are being developed to make the most of the renewable resources available, in the same way, other mature renewable energy technologies are now more efficient and their energy yield more significant.

Among the most widely used of these technologies is wind power, which has also been part of recent developments; more efficient and bigger wind turbines are now commercially available promising a significant increase in wind power production. Nevertheless, like all renewable energy resources, this method is bound to the climatic conditions of the site of the installations; the search for better resources has led this industry from onshore installations to offshore fixed-bottom ones and now, floating offshore wind turbines (FOWT) are starting to gain momentum with the beginning of the first offshore floating wind farm financed by a bank taking place just last year [12].

At the same time, new prototypes for floating structures are being considered with the objective of reducing costs and improve performance, reliability, and installation. Much of this research is accompanied by a fair share of CAD (Computer-aided design) and CAE (Computer-aided engineering) that allows for the calculation of the structures stresses and motions under a battery of circumstances, for an OFWT it is crucial to consider and simulate the behavior of the structure under a wide range of climatic conditions since the installation is constantly affected by them.

This work will describe and study the behavior of a 10MW version of the Windcrete concept, a monolithic tower structure made of concrete for offshore floating wind turbines, under the climatic conditions of two different locations. The locations considered are West of Barra and Gran Canaria Island, they will serve as a reference for severe and moderate metocean conditions respectively. All the simulations were done using the FAST software and the development of the corresponding numerical models for it will be detailed in this text.

Chapter 2

Objectives and Scope

The objective of this work is to study the motions of the structure and accelerations in the nacelle of the Windcrete concept developed for a 10MW wind turbine under five different load cases defined in the IEC 61400-3 [15] procedure (DLC 1.1, DLC 1.3, DLC 1.6, DLC 2.1, DLC 6.1) using as a reference the climatic conditions of two different locations: West of Barra and Gran Canaria Island.

The tower structure design, material, and dimensions are already defined so this work will only focus on the definition of the models used in the simulations. The 10MW reference wind turbine [3] models developed by DTU will be used for the study and in the same way, they won't be modified except for the control system that will be tuned for this structure.

All simulations were carried out using the FAST (Fatigue, Aerodynamics, Structures, and Turbulence) [18] software and therefore the models where made in this context. Using these results it will be clearer if the structure is fit to operate under the proposed conditions and this will contribute to the further development of the structure.

Chapter 3

The Energy Transition and Wind Power

Energy access is a crucial factor in the development of the economies of the countries, many of which deal with a fast-growing population. As a result, the demand for energy is increasing dramatically; from 1990 to 2016 the primary energy consumption has risen by 56%, from which in 2016, 81% came from fossil fuels (Figure 3.1). These sources have the added cost of producing greenhouse gases (GHG) emissions, which contribute to climate change. The effects of climate change are already noticeable and include increasingly frequent extreme weather events, floods, droughts, heatwaves, and the melting of the ice shields. Most projections indicate that future impact will only be more significant, and dealing with these consequences will be more expensive than preventing them.

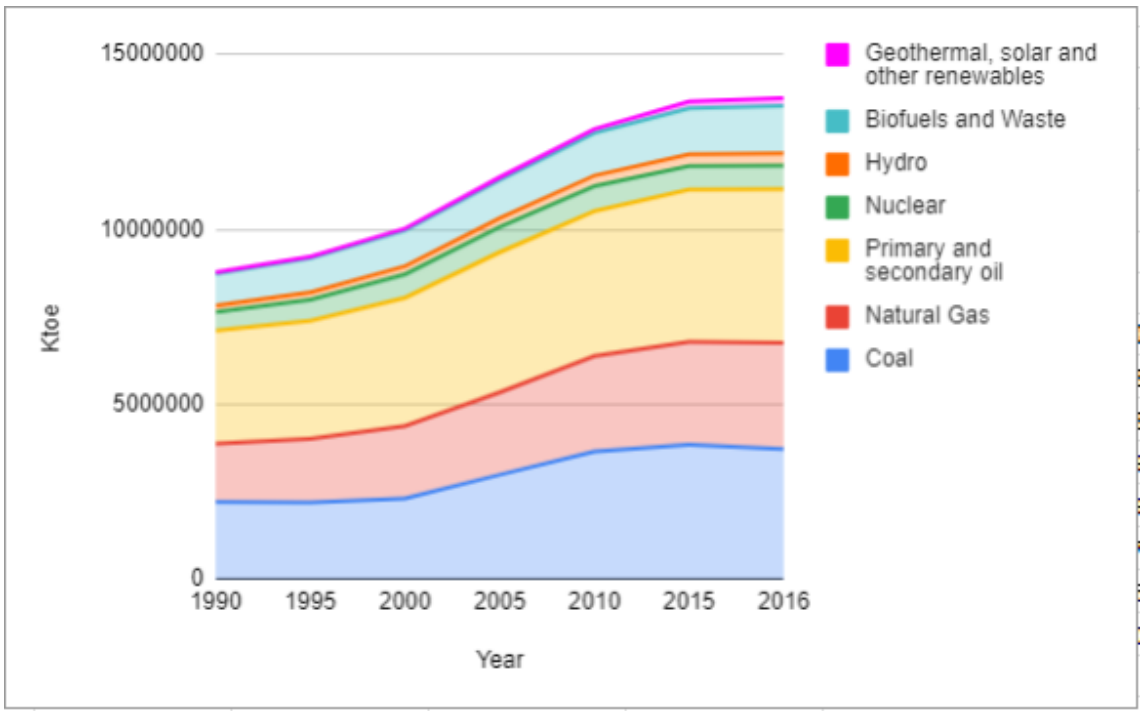

Figure 3.1: Total primary Energy Supply Consumption [14].

Therefore, considering that two-thirds of GHG emissions originate from the energy sector, the Intergovernmental Panel on Climate Change (IPCC) called for an

immediate, large-scale shift to renewable energy and energy efficiency [33].In response, many countries have adopted different agendas, including the Paris Agreement, the 2030 Agenda for Sustainable Development, and the Sendai Framework for Disaster Risk Reduction. The primary goal of the Paris Agreement is to keep the average global temperature rise well below 2 °C and as close as possible to 1.5 °C above pre-industrial levels and is the primary driver of most of the new policies related to the energy transition [36].

In 'A Roadmap to 2050' [16] the IRENA estimates that meeting the objectives of the Paris Agreement would require reduction of global energy demand through efficiency, increasing the share of renewables in the energy mix, and promoting electrification. The IRENA also indicates that renewable energies would need to comprise at least two-thirds of the total final energy supply by 2050 to achieve these goals. At the same time, the share of renewable energy in the power sector would need to increase from 25% in 2017 to 86% in 2050 [17]. It is necessary to promote the widespread use of mature technologies like solar, wind, and hydropower to achieve such a significant share of renewables in the energy mix. Furthermore, it is also necessary to invest in the development and implementation of more recent and promising technologies like offshore floating wind turbines.

Among renewable energies, wind power is the fastest-growing technology; the global wind energy production went from 3.380 GWh in 1990 to 957.694 GWh in 2016 (Figure 3.2). Since 2014, annual installations have surpassed 50 GW each year, and the Global Wind Energy Council (GWEC) expects for this trend to continue until the year 2023 for the onshore market [9]. Also, wind is one of the most extensively used renewable resources; according to the International Energy Agency (IEA) renewable energies will provide almost 30% of the total power demand in 2023, out of this percentage hydropower would be the most representative share with 16%, followed by wind (6%), solar PV (4%) and bioenergy (3%) [13].

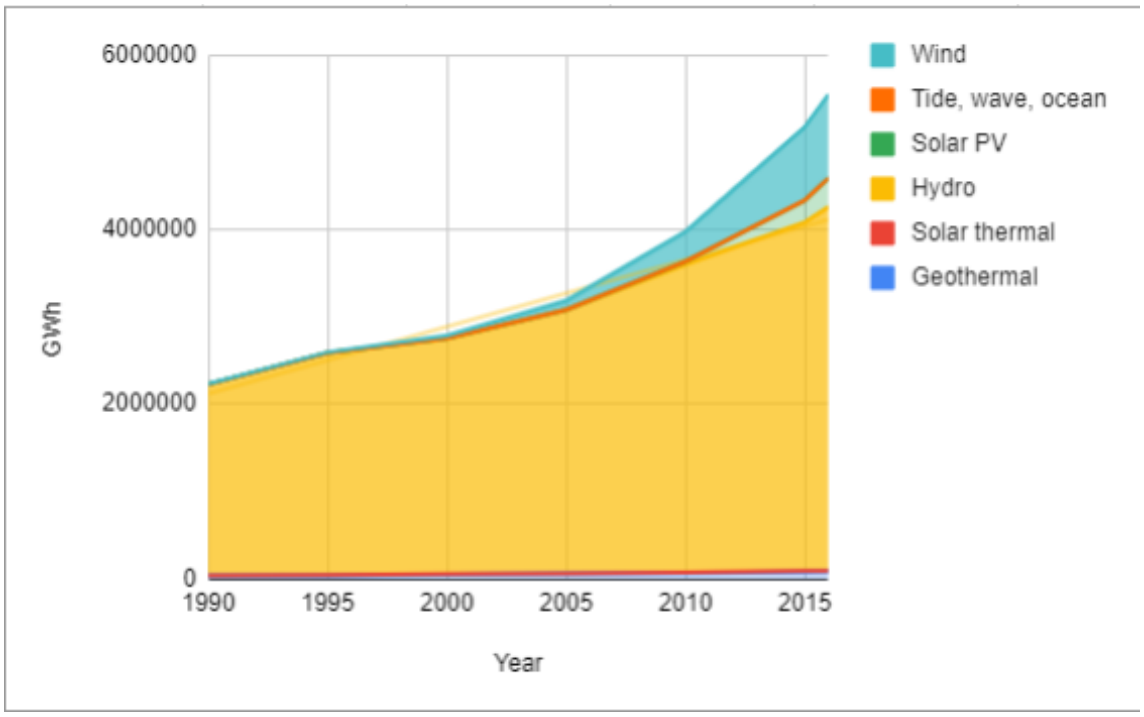

Figure 3.2: Electricity Generation from Renewable Energies[14]

Compared to other applications of renewable energy technologies, power generation through wind has an advantage because of its technological maturity and cost competitiveness [21]. Already, new solar and wind are cheap enough to outcompete oil and some gas-based generators. From the beginning of 2016 until today, reports have appeared showing a fast decrease in prices achieved in tendering processes around the world. During that year, onshore wind prices reached 30 USD/MWh in Morroco and 50 EUR/MWh for offshore wind in northern Europe [23].

There are several significant factors involved in the reduction of the Levelized Cost of Energy (LCOE) for wind power like the increase of turbine efficiency, reduction of operation and maintenance costs and improvements of the supply chain. However, in recent years, some of the main drivers of this decline have been larger swept areas (Figure 3.3) and higher hub heights, which allows for better and more cost-efficient energy production [10].

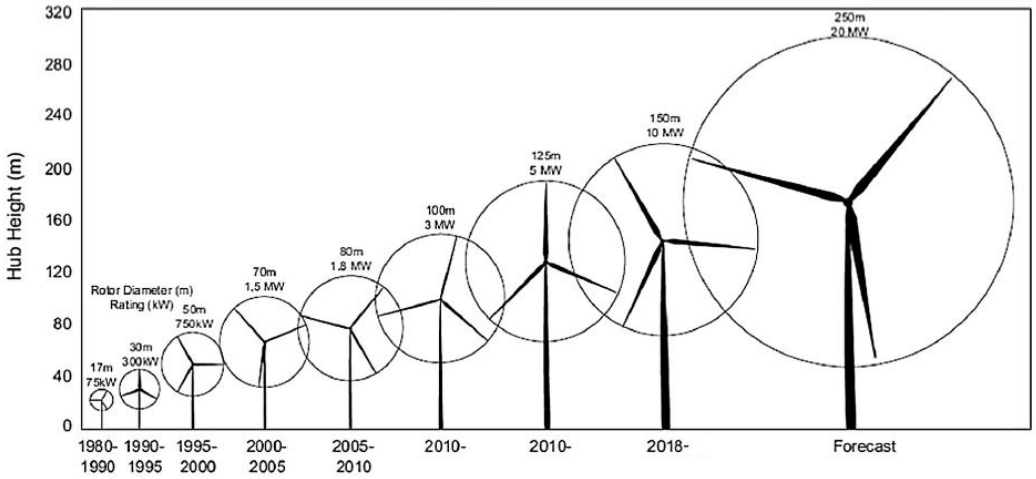

Figure 3.3: Evolution of the wind turbine swept area[37]

Nevertheless, onshore wind turbines are constrained by several factors. An onshore wind farm needs vast extensions of vacant land with a suitable wind resource; these are scarce and might interfere with other possible uses of the terrain. Also, wind turbines produce visual and noise annoyances that restrain the installation near populated areas [37]. On top of this, logistical constraints that come from the transport of components by rail or road limit the wind turbine size.

Even though the LCOE of offshore energy is currently higher than onshore wind power (Figure 3.4), this technology has several advantages, mainly that the offshore wind resource can be between 1.2 to 2 times faster and the energy yield generally increases by going further from land [22]. Also, the resource is more consistent, with less turbulence intensity and smaller shear compared to the resource onshore. If constructed near the coastline, the size of the wind turbine is not limited by transport routes and there are vast expanse of uninterrupted open sea for this installations.

With this in mind, some of the investment and research has shifted to offshore installations, mainly in Europe where the shallow water wind resource is more available. However, so far the energy prices produced from fixed-bottom offshore wind turbines are not competitive compared to other traditional energy sources. Offshore wind power lead times are usually longer; also, grid connection, installation, and construction costs are higher and very dependent on geographic factors like water

depth and distance to the shore.

A higher capital investment is required for an offshore wind turbine because of the costs associated with marinization of the turbine and the added complications of the support structure, installation and decommissioning. Furthermore, offshore installations are less accessible than onshore installations which raise the operations and maintenance costs and possibly increase the downtime of the machines. Not only do offshore wind turbines experience environmental loading from wind, but they must also withstand other conditions such as hydrodynamic loading from waves and sea currents. As a result the complexity of the design increases.

Nevertheless, in the same way as onshore wind power, cost reductions have commenced with the industrialization and standardization of the manufacturing and installation methods. The improvement in capacity factors and energy yield that come with the use of more powerful turbines further from the mainland might mitigate the higher capital and operational expenditures of an offshore project. Nonetheless, water depth is a limiting factor for offshore wind installations; in 2016 the average water depth of completed, or partially completed, wind farms was 29 meters, with an average distance to the nearest port of 44 km [39].

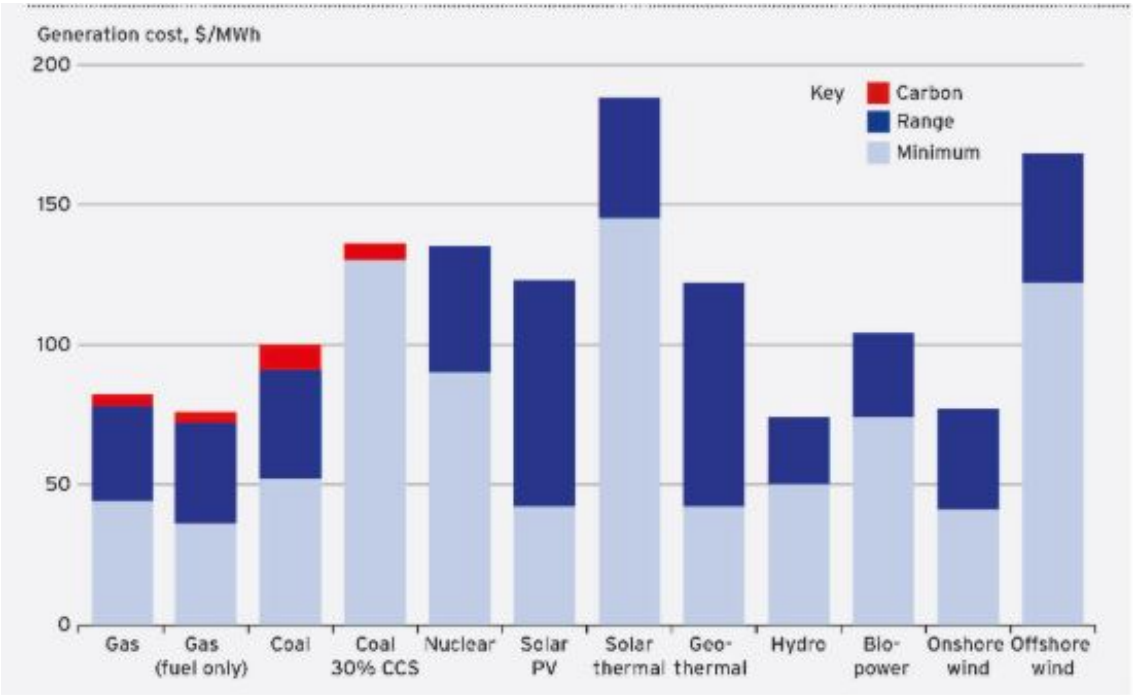

Figure 3.4: Generation Costs for Different Technologies [1]

Chapter 4

Floating Offshore Wind Turbines

For fixed bottom offshore wind turbines higher water depth means a more complex construction, installation process and a more expensive structures. At the same time, in many occasions the best wind resource is usually located in places with water depths that might out of reach for these structures. Much of the offshore wind resource potential in the United States, China, Japan, Norway, and many other countries is available in water deeper than 30 m. For example, the wind resource potential at 9 to 90 kilometers off the U.S. coast is estimated to be more than the total currently installed electricity-generating capacity of the United States (more than 900,000 MW when accounting for exclusions) [28].

For locations with water depths above 45m offshore floating wind turbines are a solution that is worth considering since foundation and installations cost reductions can be expected; since these structures don't need to reach the seabed there is a significant reduction in material costs and structural mass.

In a floating offshore wind turbine (FOWT) the structure is linked to the seabed by a mooring system instead of a solid structure. There are several proposals for this constructions but so far most of them can be classified as one of three main kind of FOWT being used for floating installations, these are:

- **Semi-submersible platform**: The platform is a semi-submerged buoyant structure anchored to the seabed with catenary mooring lines. This often requires a heavy structure to provide stability but at the same time allows for a low draft which simplifies the logistics of transport and installation.

- **Spar Buoy**: The platform is a cylindrical ballast in which the center of gravity is lower that the center of buoyancy, this provides stability. The structure is also anchored to the seabed using catenary moorings. The structure is usually fairly simple and easy to fabricate but the large draft might produce assembly, transportation and installation problems; it also confines the installation to large water depths (>100 m) since a large part of the platform needs to be underwater.

- **Tension leg platform**: In this case a semi-submerged floating structure is also used but it is anchored with tensioned mooring lines. The tension provided by the mooring lines makes the structure more stable and allows for smaller drafts in comparison to a semi-submersible platform. On the other hand installation challenges are significant and there is a significant operational risk if a tendon fails.

In the following table (Table 4.1) the advantages and disadvantages of each structure are described for easier comparison. Also, the described FOWT are illustrated in figure 4.1.

Typology	Strengths	Weaknesses
Semi-submersible	• Flexible application due to the ability to operate in shallow water depths. • Low vessel requirement - only tug boats required. • Onshore turbine assembly. • Amenable to port-side major repairs	• High structural mass to provide sufficient buoyancy and stability. • Complex steel structures with many welded joint can be difficult to fabricate. • Potentially costly active ballast systems.
Spar-buoy	• Simple design is amenable to serial fabrication processes • Few moving parts (no active ballast required) • Excellent stability	• Constrained to deep water locations • Offshore turbine assembly requires dynamic positioning vessels and heavy lift cranes • Large draft limits ability to tow the structure back to port for major repairs.
Tension leg platform	• Low structural mass • Onshore turbine stability assembly Few moving parts (no active ballast required) • Excellent stability	• High loads on the mooring and anchoring system • Challenging installation process • Bespoke installation barge often required.

Table 4.1: Comparison of the Main Kinds of FOWT [1].

Figure 4.1: Floating Wind Foundation Typologies [1].

As mentioned before FOWT could be a great option for deep water locations, nevertheless it is still uncertain how significant the economical advantage will be, the technology is still too immature and there are very few operating windfamrs and prototypes. In terms of capital costs the foundation and installation costs are expected to be significantly lower than in a fixed-bottom offshore wind installation, nevertheless once the added costs of the mooring system is considered that the total capital expenditure might be higher for FOWT. In terms of operative costs the routine maintenance operations should be the similar to those of a fixed-bottom structure, but bigger operations like the replacement of the gearbox would be more affordable since is possible take the turbine to a port for reparations. Taking this into account and the higher capacity factors associated with FOWT the levelized cost of energy for this kind of structures should be slightly lower than for fixed bottom wind turbines in the future.

It must be taken into account that this is not the first time that the transition from fixed bottom to floating structures is made, much of the experience in this field comes from the oil and gas industry, in which significant cost reduction was achieved trough standardised designs (figure 4.2), optimised fabrication lines on top of the advantages mentioned above in terms of installation and overall structure. The same scenario is also valid for the offshore floating wind industry.

4.1 Motions of a Floating Offshore Wind Turbine

A FOWT is able to move in all six degrees of freedom, the tree translation movements are called sway, heave and surge. The tree rotational movements are called pitch,

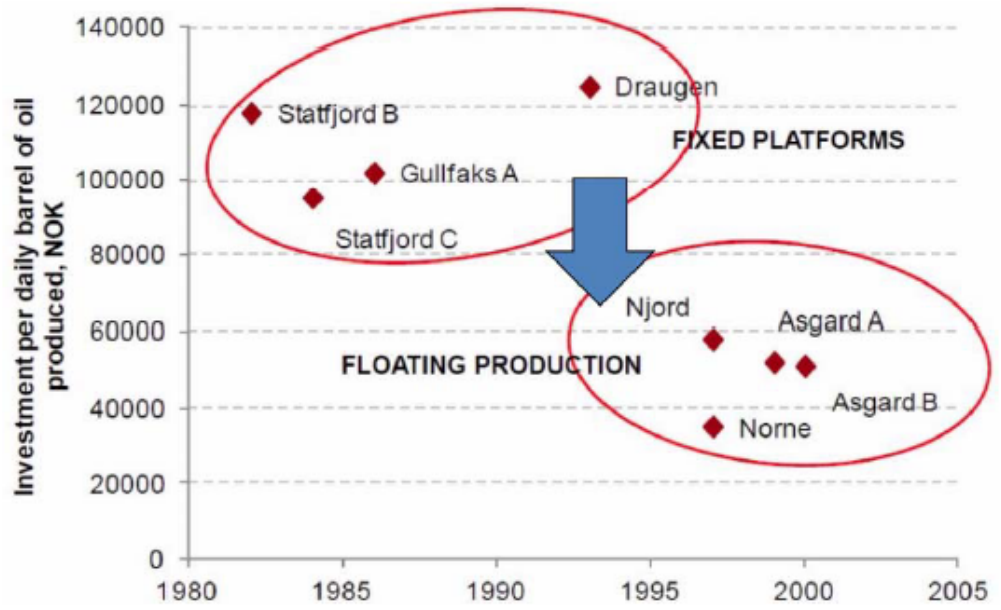

Figure 4.2: Cost reductions in oil production using floating platforms [1].

roll and yaw. These motions are shown in figure 4.3.

To ensure the proper operation of the Windcrete concept during its lifespan in each location the motion and acceleration limits presented in table 4.2 will be used:

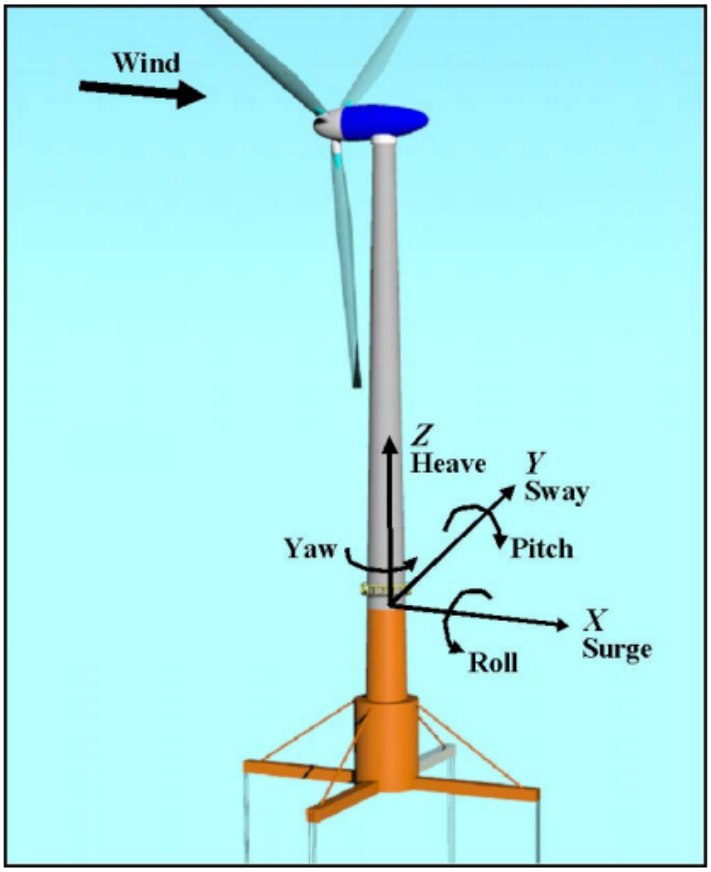

Figure 4.3: Degrees of Freedom of a FOWT. [19]

DoF/Limit typology	Limit
Operation	
Yaw (max)	[-15°,+15°]
Yaw (10 min. std)	<3°
Pitch (max)	[-5.5°,+5.5°]
Pitch (10 min. average)	[-4°,+4°]
Roll (max)	[-3.5°,+3.5°]
Pitch/Roll (10 min. std)	<1°
Idling Condition	
Pitch (max)	[-7°,+7°]
Pitch (10 min. average)	[-5°,+5°]
Emergency Stop	
Pitch (max)	[-15°,+15°]
Excursion Restrictions	
Horizontal offset (mean during operation conditions)	15m
Horizontal offset (max. during parked conditions)	30m
Acceleration Limits (Nacelle)	
Operation	2.8m/s^2
Survival	3.5m/s^2

Table 4.2: Motion and acceleration limits for a FOWT.

Chapter 5

FAST Software and Modules

The FAST (Fatigue, Aerodynamics, structures, turbulence) code is a simulator developed by the National Renewable Energy Laboratory (NREL) that is capable of simulating the couple dynamic response of a wide configuration of wind turbines including onshore, offshore fixed bottom and offshore floating wind turbines. Since the 8th version of this software, NREL have implemented a modularized system in which each module deals with a different part of the physical model, including aerodynamic, hydrodynamic, control and electrical systems models; figure 5.1 shows the control volumes associated with each module for floating offshore wind turbines. In order to understand the context in which the Windcrete tower models where developed a brief outline of each used modules will be given in this chapter.

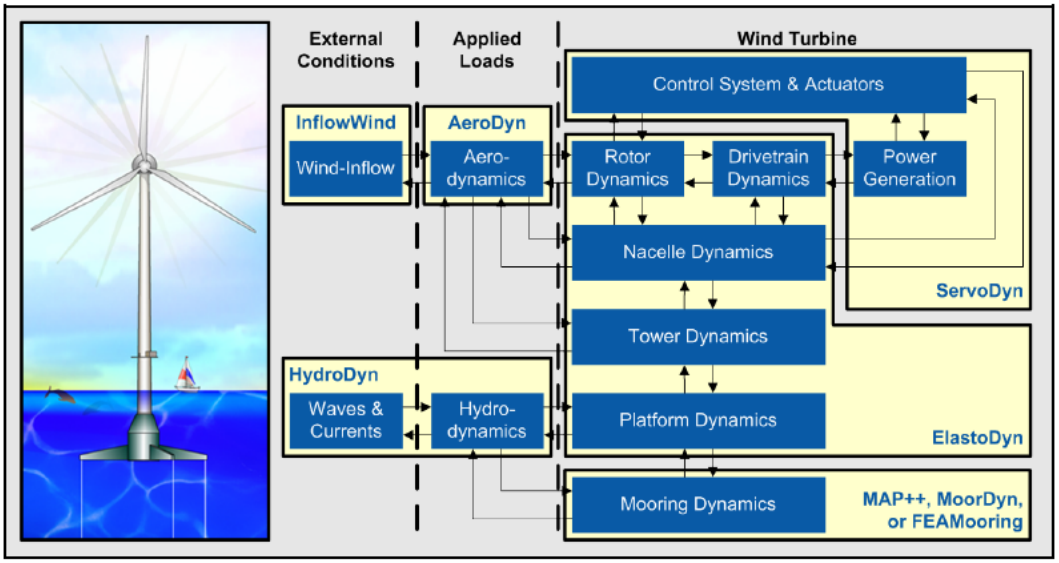

Figure 5.1: FAST Control Volumes for floating systems[18].

5.1 AeroDyn

Is a time domain wind turbine aerodynamics module that is able to calculate the aerodynamic loads both on the blades and the tower these calculations are based on the principles of actuator lines where a three dimensional flow around the body

is approximated in a series of two dimensional cross sections along the body of the tower or the blades. Aerodyn assumes that the geometry of the structure consist of a rotor with a range from one to three blades over a singles straight, vertical, and undeflected tower. When coupled to FAST this module receives the instantaneous structural position, orientation and velocities of the nodes of the blades, hub and tower for its calculations. For this particular case the aerodynamic loads on the tower where not calculated, this is because the models developed for the DTU 10 MW wind turbine used Aerodyn V14 which does not include this option.The wind itself is generated by another module called inflow-wind.

5.2 HydroDyn

HydroDyn allows for the calculation of the time-domain hydrodynamic loads over a fixed-bottom or floating offshore wind turbine, it can use potential-flow theory, strip theory or a combination of both solutions. This module also generates the waves used in the study which can be regular (periodic) or irregular (stochastic). The potential flow solution requires frequency dependent hydrodynamic coefficients and must supplied by a separate frequency domain panel code (e,g WAMIT). The strip theory solution can be applied across multiple interconnected members and are derived directly from undisturbed wave and current kinematics; the strip theory loads include the relative form of Morrison equation for the disturbed fluid inertia, added mass and viscous drag components, additional distributed load components include axial loads and static buoyancy loads. The hydrodynamic coefficients required for this solution come trough user specified dynamic-pressure, added-mass, and viscous drag coefficients.

5.3 ServoDyn

Includes control and electrical-drive models for blade pitch, generator torque, nacelle yaw, high-speed shaft brake, and blade-tip brakes. This module uses the structural motions, reaction loads and wind measurements to define the controller commands for the proper function of the wind turbine. The control routines come from a separated sub-routines that can be provided by Matlab, Simulink or a fortran subroutine.

5.4 MoorDyn

MoorDyn is meant to be used in conjunction with another program that tells it how the fairlead ends of the mooring lines are moving. With this input the module is capable of predicting the dynamic loads of the mooring system and calculating tensions and forces in the lines. This forces will also affect the movement of the floating wind turbine.

5.5 ElastoDyn

ElastoDyn uses the structural models of the rotor, drivetrain, nacelle, tower, and platform to calculate the displacements, velocities, accelerations and reaction loads of each component, taking as input the aerodynamic and hydrodynamic loads from other modules and the control commands from Servodyn.

Chapter 6

Description of the Windcrete Concept

Windcrete, shown in figure 6.1, is a spar type structure concept for floating offshore wind turbines developed by a research team from the Polytechnic University of Catalonia. It consist on a monolithic structure mainly made of concrete instead of steel like most commercial structures [2].

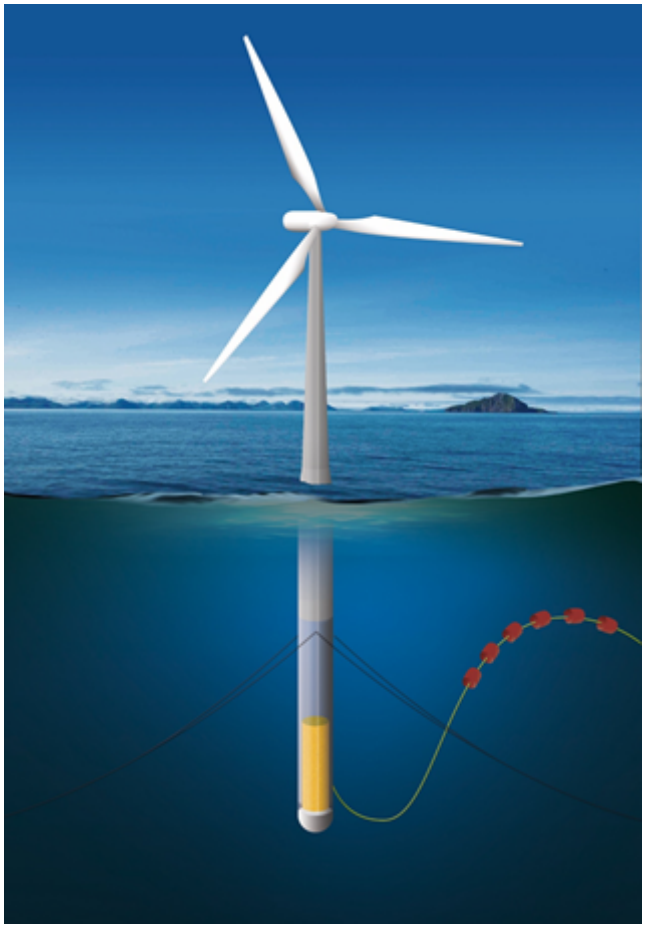

Figure 6.1: Windcrete Floating Offshore Wind Turbine

The effectiveness and advantages of the use of concrete for offshore structures have been already proven in the oil and gas industry, from the experience of this

sector, the FIB [7] has reached the following conclusions about the use of concrete in offshore structures:

- Concrete offshore platforms provide full operational safety.
- They show a very high durability level.
- They do not require costly maintenance and repair operations.
- Their effective lifespan has been underestimated and their 20-year initial design life can be greatly extended.

Taking this into account a structure made of concrete could greatly reduce operation expenditures as the maintenance operations would be minimized, also, the lifetime of a tower structure could greatly exceed the lifespan of the turbine, for some structures, a lifetime longer than 60 years can be expected, so the tower could be used for another turbine in the future.

On the other hand the use of a monolithic structure contributes the the durability of the structure minimising the penetration of chlorides, water and soon, and preventing damage such as that detected in the transitions zones of mixed concrete and steel structures. Also, durability and fatigue problems that have been detected in the transition zones between the steel of the tower and the concrete of the foundation in several bottom-fixed offshore wind farms could be avoided with this construction method. Currently, concept upgrades to 10MW and 15WM are being worked on, in this work the focus point will be the structure developed for 10MW wind turbines.

Chapter 7

Description of the DTU 10MW Reference Wind Turbine

The DTU 10MW Reference Wind Turbine, was originally developed through cooperation between DTU Wind Energy and Vestas with the Light Rotor project .The model was developed with the objective providing a publicly available representative design basis for the next generation of new optimized rotors. The turbine is a three-bladed upwind wind turbine with a rated power of 10MW, in table 7.1 more specific details about the turbine model will be given.

For this work the available data of the turbine and blades system were used without modifications therefore their specific characteristics wont be presented but are available in the reports by LIFE50+. In the case of the control system a modified version of the system developed for the Nautilus wind turbine was defined in this work, this will be explained in following chapters.

Rotor Orientation	Clockwise rotation - Upwind
Control	Variable Speed, Collective Pitch
Cut in wind speed [m/s]	4
Cut out wind speed [m/s]	25
Rated wind speed [m/s]	11.4
Rated power [MW]	10.0
Number of blades	3
Rotor diameter [m]	178.3
Hub diameter [m]	5.6
Hub height [m]	119
Drivetrain	Medium speed, multiple stage gear box
Minimum rotor speed [m/s]	6.0
Gearbox ratio	50
Hub overhang [m]	7.1
Shaft tilt angle [deg]	5.0
Rotor precone angle [deg]	-2.5
Blade prebend [m]	3.332
Rotor mass [Kg]	227962
Nacelle mass [Kg]	446036

Table 7.1: 10MW Reference wind turbine properties [25].

Chapter 8

Climate Conditions

For this work the the motions and accelerations of the Windcrete concept were studied under the metocean conditions of two locations, West of Barra and Gran Canaria, wich present severe and moderate conditions respectively. The data obtained from this sites will define the conditions for the simulation of each DLC.

8.1 Site A: West of Barra (Severe Met-ocean Conditions)

The simulations and load cases in this section are all defined using as reference the met-ocean conditions for West of Barra in Scotland. This site has been selected by protects like LIFES50+ [31] as an area with severe met-ocean conditions. The site is located 19km west of Barra island and its been recognized as a potential location for future FOWT projects.

8.1.1 Wind Climate

The wind data from this reference was measured on 1-hour average speed at 10 m above MSL, according tho the LIFES50+ deliverable 1.1 report [31] the most reliable method to extrapolate the wind speed data to the target height in operating conditions is the use of the logarithmic law (Equation 8.1) considering Zo=0,0002 so it was used to estimate the wind speeds at hub height, presented in table 8.1.

$$V(z) = V_{hub}\frac{ln(z/z_o)}{ln(z_{hub}/z_o)} \tag{8.1}$$

On the other hand for extreme wind conditions a power law (equation 8.2) relationship with $\alpha = 0{,}12$ was used. The extreme wind speed (V_{ref}), is defined as the value of the highest wind speed, averaged over 10 minutes, with an annual exceeding probability of 2% (50 years return period). In order to estimate the V_{ref} value it is necessary to use a method that extrapolates the horizon of the extreme wind speed prediction to 50 years, in this case the EWTSII method was used, the obtained result is presented in table. 8.2.

$$V(z) = V_{hub}(z/z_{hub})^{\alpha} \tag{8.2}$$

@Hub Height	@10m
4	3.255
6	4.882
8	6.510
10	8.137
12	9.765
14	11.392
16	13.020
18	14.647
20	16.274
22	17.902
24	19.530
25	20.344

Table 8.1: Wind Speeds at hub height and 10m above MSL [31].

@10m	@Hub Height
38.25	53.79

Table 8.2: 50 years return wind speed at hub height and 10m above MSL [31].

Wave Climate

For the case of wave climate the main focus is the wave height and peak period in relation to the wind speed. The deliverable 1.1 report by LIFES50+ [31] used the data in table 8.1 to develop a reliable formula that could predict the wave height as a function of the wind speed, as a result a third order polynomial equation (Eq. 8.3) was developed, where u is the wind speed at 10 meters.

Hs [m]	Mean Wind Speed at 10 [m/s]											
	0.00-0.30	0.30-1.60	1.60-3.40	3.40-5.50	5.50-8.00	8.00-10.80	10.80-13.90	13.90-17.20	17.20-20.80	20.80-24.50	24.50-28.50	28.50-32.70
0.0-0.5						1						
0.5-1.0		5	1054	2316	897	14	1					
1.0-1.5		14	1061	4055	5701	1444	9					
1.5-2.0		1	632	2070	5126	4736	335	1				
2.0-2.5		3	284	1083	3024	5167	1809	21				
2.5-3.0			139	468	1570	3645	2933	163				
3.0-3.5			58	197	762	2080	2981	550	3			
3.5-4.0			40	119	398	1190	2586	997	21			
4.0-4.5			4	33	193	747	2157	1324	96			
4.5-5.0			2	10	81	409	1441	1418	164			
5.0-5.5			1	10	32	184	767	1180	301	6		
5.5-6.0				1	22	87	452	869	370	21		
6.0-6.5					4	39	207	532	320	25		
6.5-7.0					3	12	116	463	334	24		
7.0-7.5						12	64	278	194	31	1	
7.5-8.0						2	38	195	137	44		
8.0-8.5						2	22	152	138	33	3	
8.5-9.0						2	10	98	201	45	3	
9.0-13.5							6	108	458	258	79	2

Figure 8.1: Wind- Wave Combined Distribution: Hs-u10 Correlation [31].

$$Hs(u) = 0.0079u^3 - 0.2499u^2 + 3.4366u + 1.9859 \tag{8.3}$$

In the same way a relation (Eq. 8.4) between the significant wave height and peak period was obtained using the available data for the site presented in table 8.2. This relation was also used to estimate the peak period for the 50 years return significant wave height presented in table 8.3.

Hs [m]	Tp[s]																
	2-3	3-4	4-5	5-6	6-7	7-8	8-9	9-10	10-11	11-12	12-13	13-14	14-15	15-16	16-17	17-18	18-19
0.0-0.5	1																
0.5-1.0		129	337	681	581	1242	774	341	88	24	11	40	28	11			
1.0-1.5		18	589	1721	1189	2403	3333	1824	754	284	120	23	20	6			
1.5-2.0			21	1260	1855	1644	2765	2720	1444	744	235	131	50	27	3	2	
2.0-2.5		1	4	164	1804	1614	1843	2055	1773	1273	562	222	40	31		4	1
2.5-3.0			1	8	607	1536	1290	1462	1659	1184	686	338	101	40	1	8	3
3.0-3.5					85	989	970	1014	1170	1140	749	265	167	61	11	9	1
3.5-4.0					10	397	846	859	971	873	754	319	221	76	20	5	
4.0-4.5					1	53	646	706	744	893	791	353	206	127	30	4	
4.5-5.0						8	221	529	586	790	659	414	167	76	44	27	4
5.0-5.5							44	340	558	517	441	250	252	56	9	10	4
5.5-6.0							7	169	293	433	424	214	182	75	9	16	
6.0-6.5							1	67	101	315	263	186	100	54	21	13	6
6.5-7.0								3	42	220	301	218	101	35	17	13	2
7.0-7.5									15	106	160	156	69	54	17	1	
7.5-8.0									8	32	145	117	59	50	1	4	
8.0-8.5										10	121	112	67	37		3	
8.5-9.0										3	115	148	62	25	4	2	
9.0-13.5											78	277	321	197	15	21	

Figure 8.2: Significant Wave Height – Peak Period Frequency [31].

$$T_p(H_s) = 3.1338ln(H_s) + 6.7566 \tag{8.4}$$

@Hs	@Tp
15.6	15.37

Table 8.3: 50 Years Return Wave Height [31].

Using relations 8.3 and 8.4 it was possible to obtain the significant wave heights and peak periods for the wind speeds considered for the design load cases, these are presented in table 8.4.

8.2 Site B: Gran Canaria Island (Moderate Met-ocean Conditions)

The site is located south east of the Gran Canaria Island and its conditions will be used as a reference for moderate met-ocean conditions in this work. This site wind and wave data is taken from the Spanish Ports Authority for the following coordinates:

15°19'48.00" W 27°45'0.00" N

8.2.1 Wind Climate

The wind conditions for Gran Canaria were taken from a report developed by Core Wind that calculates the normal and extreme wind profile using also equations 8.1

@Hub Height	@10m	Hs [m]	Tp [s]
4	3.255	0.64	2.5
6	4.882	0.92	7.25
8	6.510	1.34	7.68
10	8.137	1.92	8.80
12	9.765	2.64	9.80
14	11.392	3.52	10.70
16	13.020	4.54	11.50
18	14.647	5.72	12.22
20	16.274	7.04	12.87
22	17.902	8.52	13.47
24	19.530	10.14	14.12
25	20.344	11.00	14.27

Table 8.4: Wind and Wave Climate conditions for operational range

Hs [m]	Mean Wind Speed at 10 [m/s]										
	0.00-2.00	2.00-4.00	4.00-6.00	6.00-8.00	8.00-10.00	10.00-12.00	12.00-14.00	14.00-16.00	16.00-18.00	18.00-20.00	>20.00
0.0-1.0	2.083	8.396	12.354	8.754	4.174	1.685	0.588	0.144	0.044	0.01	0.001
1.0-2.0	3.012	12.063	18.533	12.298	5.582	2.195	0.777	0.248	0.062	0.01	0.006
2.0-3.0	0.384	1.387	2.041	1.568	0.785	0.295	0.126	0.055	0.012	0.003	0.002
3.0-4.0	0.014	0.06	0.109	0.076	0.034	0.009	0.007	0.003			
4.0-5.0			0.005	0.003							
5.0-6.0											
6.0-7.0											
>7.0											

Figure 8.3: Specific wave height in relation to the wind speed @10m [6].

and 8.2 respectively. The report also estimates the 50 year return wind speed at 119 meters (hub height) as 40.07m/s.

8.2.2 Wave Climate

The data presented by the Corewind report concerning the relation of the wind speed, waves specific height and period is presented in the figures 8.3 and 8.4.

From figure 8.3 it can be appreciated that the most common specific wave height for each wind speed range is between 1m and 2m, so a conservative approach would be to use 2m as the H_s and a 6s T_p (from figure 8.4) for for every wind speed while in NSS. On the other hand, the CoreWind report states hat the 50 year return wave has a specific height of 5.11m and a peak period of 9s.

Tp [s]	Significant Wave Height [m]				
	0.00-1.00	1.00-2.00	2.00-3.00	3.00-4.00	4.00-5.00
1.0-2.0	0.037	0.001			
2.0-3.0	0.771	0.3			
3.0-4.0	2.603	1.845			
4.0-5.0	4.524	5.132	0.003		
5.0-6.0	5.392	10.973	0.049		
6.0-7.0	4.907	14.608	0.465		
7.0-8.0	4.211	9.569	2.593	0.012	
8.0-9.0	3.504	5.006	2.552	0.11	
9.0-10.0	2.836	3.119	1.087	0.147	0.001
10.0-11.	2.252	1.865	0.522	0.073	0.003
11.0-12.0	1.766	1.25	0.275	0.028	
12.0-13.0	1.244	0.823	0.161	0.005	
13.0-14.0	0.827	0.542	0.12	0.001	
14.0-15.0	0.512	0.326	0.085	0.002	
15.0-16.0	0.27	0.21	0.052	0.003	
16.0-17.0	0.129	0.119	0.034	0.002	
17.0-18.0	0.04	0.058	0.005		
18.0-19.0	0.01	0.018	0		
19.0-20.0	0.001	0.006	0.001		
20.0-21.0		0.002			
21.0-22.0		0.001			

Figure 8.4: Peak Period in Relation to the Specific Wave Height [6].

Chapter 9

Load Cases

The design load cases (DLC) [15] are used to define situations that the wind turbine might face during its lifespan in order to verify the structural integrity of the wind turbine and its parts. These include the climate conditions found in the site of the installation that the wind turbine will face under under normal operation, start up, shut down, occurrences or faults and a parked. The cases evaluated in this work wont cover start up nor shutdown of the wind turbine.

- **DLC 1.1**: In this design situation, the wind turbine is in operation and connected to the electrical grid while the control system is active, fault situations are not included in this load case. For the wind climate conditions, they must be considered from the cut-in to cut out wind speed with intervals that must be smaller than 2m/s. Also, the loads related to atmospheric turbulence must be considered using a normal turbulence model (NTM). For this DLC irregular normal sea state (NSS) conditions must be assumed in which the wind speed will dictate the significant wave height and peak spectral period. For this simulation 6 seeds will be used for each wind speed and the simulation duration will be 600s.

- **DLC 1.3**: For this case the turbine will be operational under the same conditions as in DLC 1.1 but the wind model will be a an extreme turbulence model (ETM), also this simulation must have a duration of at least 1500s.

- **DLC 1.6**: As in the load case 1.1 the turbine will operate under a NTM wind that covers all the operational range, for the waves specific height and period the IEC requires the use of a severe sea state wave climate, in these data in unavailable a conservative option is to use the 50 years return wave specific height and period. For this DLC at least 3600s of simulation are required and for this work the 50 year return wave data will be used.

- **DLC 2.1**: The turbine will operate normally under NTM wind and NSS wave climates. After the first 10s of the simulation a grid loss or control fault must be induced. This will be achieved turning the pitch angle of the blades to 90 degrees with a speed superior to 8 °/s. The simulations must be at least 600s long.

- **DLC 6.1**: In this design situation the turbine is parked and subdued to 50 year return wind speed and wave specific height and period. For this simulations a time of 3600s will be used.

Chapter 10

Numerical Models of the 10 MW Windcrete

In order to get reliable results from the simulation the numerical models of the structure must represent the behaviour of the tower in a accurate way, in this chapter the physical properties of the different sections of the tower structure (tower, platform and moorings) will be described.

10.1 Tower

When the wind turbine is at equilibrium position the tower section of the structure starts at MSL and it consist of a conical, hollow structure made of concrete that connects the floating platform an the rotor nacelle assembly. The tower properties are shown in table 10.1

The physical properties of the tower where calculated using a CAD model of the tower section, on the other hand for the calculation of the natural frequencies and mode shapes the Bmodes [8] module was used and, therefore, a simplified model of the structure had to be defined. For the model the conical structure was approximated using thirty cylindrical sections (as show in figure 10.1) of equal height and constant wall thickness, the radius of each cylinder was determined linearly interpolating between the base and the top outer radius. The obtained natural frequencies are displayed in table 10.1 and the mode shapes for the first two vibrations modes can be seen in figure 10.2, where the displacements of the tower are shown in relation to the unitary length of the ladder for the first two natural frequencies.

10.2 Platform

The platform section consist of a hollow cylindrical structure that joins the tower section though a conical transition part, the structure is partially filled with ballast (figure 10.3), this brings down the center of mass of the structure since most of the material is at the bottom of it. The characteristics of this section are shown in table 10.2.

The platform section of the tower suffers all loads from the interaction with water, these are calculated using the strip theory solution of the HydroDyn module. To define the hydrodynamic coefficients of a structure dedicated softwares like WAMIT

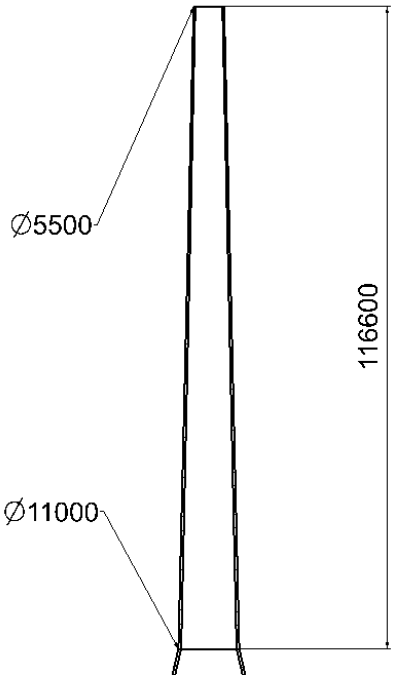

(a) Windcrete Tower CAD Model Dimensions.

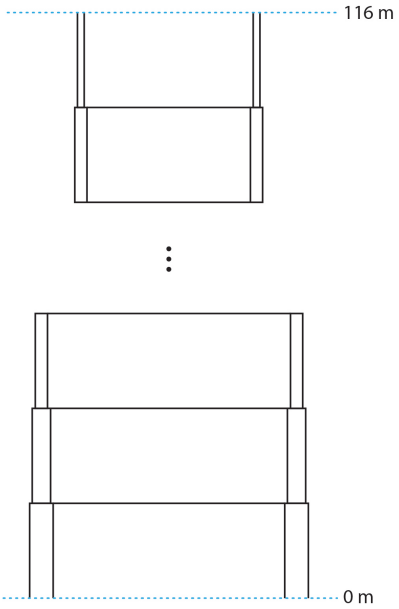

(b) Windcrete Tower Approximation for FAST.

Figure 10.1: Tower Model Definition

Property	Unit	Value
Tower base elevation above MSL	[m]	0
Tower base diameter	[m]	11
Tower base wall thickness	[m]	0.5
Tower top elevation above MSL	[m]	116.6
Tower top diameter	[m]	5.5
Tower wall average thickness	[m]	0.4
Total mass	[Kg]	2365139.65
Inertia about x,y axis w.r.t. tower-CM	[Kgm^2]	2467.859
1st fore-aft natural frequency (clamped tower)	[Hz]	0.44075
2nd fore-aft natural frequency (clamped tower)	[Hz]	2.453
1st side-side natural frequency (clamped tower)	[Hz]	0.44075
2nd side-side natural frequency (clamped tower)	[Hz]	2.453
Density	[Kg/m^3]	2000
Modulus of elasticity	[GPa]	21
Shear modulus of elasticity	[GPa]	36

Table 10.1: Physical Properties of the Tower

[4] are usually employed; also, scale models can be used to study their response in the water to obtain the coefficients for the original structure.

In the case of this work, the values of the hydrodinamic coefficients of the structure where taken from a previous study done for a scale model of a 5MW version of the windcrete concept. For the calculation of the linear hydrostatic restoring matrix the following formulas where used:

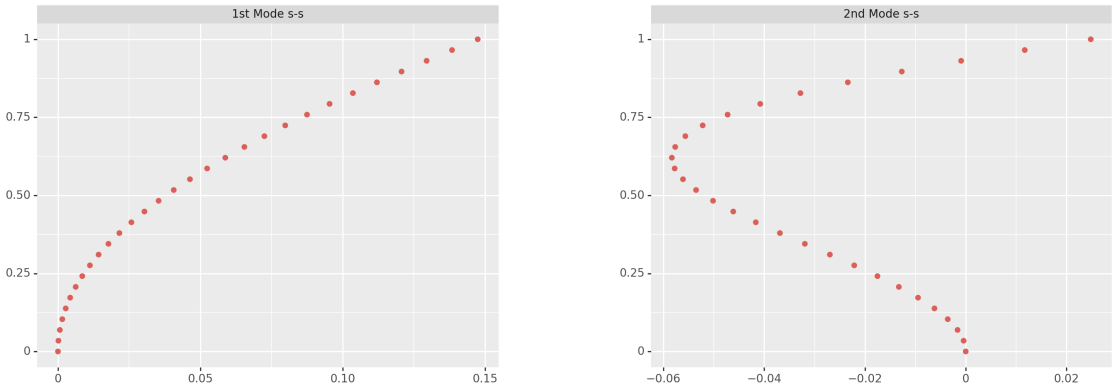

(a) 1st Mode s-s (b) 2nd Mode s-s

Figure 10.2: Tower Vibration Modes

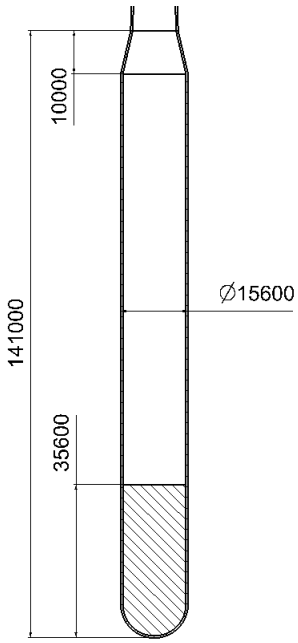

Figure 10.3: Windcrete Platform CAD Model Dimensions.

Property	Unit	Value
Draft	[m]	141
Platform Diameter	[m]	15.6
Transition section length	[m]	10
Transition section top diameter	[m]	11
Ballast Mass	[Kg]	16406716.306
Ballast Density	[Kg/m^3]	3000
Platform Center of Mass	[m]	107.23
Platform x,y inertia	[Kgm^2]	24669727344.68

Table 10.2: Platform Characteristics

$$C_{33} = \rho g A_0 \tag{10.1}$$

$$C_{34} = C_{43} = \rho g \iint_{A_0} y \, dA \tag{10.2}$$

$$C_{35} = C_{53} = -\rho g \iint_{A_0} x \, dA \tag{10.3}$$

$$C_{44} = \rho g \iint_{A_0} y^2 \, dA + \rho g V_0 z_b - m_{mg} g z_{mg} - m_f g z_f \tag{10.4}$$

$$C_{45} = C_{54} = -\rho g \iint_{A_0} xy \, dA \tag{10.5}$$

$$C_{46} = -\rho g V_0 x_b + m_{mg} g x_{mg} + m_f g x_f \tag{10.6}$$

$$C_{55} = \rho g \iint_{A_0} x^2 \, dA + \rho g V_0 z_b - m_{mg} g z_{mg} - m_f g z_f \tag{10.7}$$

$$C_{56} = -\rho g V_0 y_b + m_{mg} g y_{mg} + m_f g y_f \tag{10.8}$$

$$\begin{bmatrix} 0 & 0 & 0 & 0 & 0 & 0 \\ 0 & 0 & 0 & 0 & 0 & 0 \\ 0 & 0 & C_{33} & C_{34} & C_{35} & 0 \\ 0 & 0 & C_{43} & C_{44} & C_{45} & C_{46} \\ 0 & 0 & C_{53} & C_{54} & C_{55} & C_{56} \\ 0 & 0 & 0 & 0 & 0 & 0 \end{bmatrix} = \begin{bmatrix} 0 & 0 & 0 & 0 & 0 & 0 \\ 0 & 0 & 0 & 0 & 0 & 0 \\ 0 & 0 & 9.32x10^5 & 0 & 0 & 0 \\ 0 & 0 & 0 & -1.9073x10^{10} & 0 & 0 \\ 0 & 0 & 0 & 0 & -1.9073x10^{10} & 0 \\ 0 & 0 & 0 & 0 & 0 & 0 \end{bmatrix} \tag{10.9}$$

where:

ρ water density, kg/m^3

g gravity, m/s2

A_0 undisplaced waterplane area of platform, m^2

V_0 undisplaced volume of platform, m^3

$(x_b, y_b.z_b)$ coordinates of the center of buoyancy of the undisplaced platform, m

m_{mg} total mass of marine growth, kg

(x_{mg}, y_{mg}, z_{mg}) coordinates of the center of mass of the undisplaced marine growth mass, m

m_f total mass of ballasting/flooding, kg

(x_f, y_f, z_f) coordinates of the center of mass of the undisplaced filled fluid (flooding or ballasting) mass, m

For each case the origin of the coordinate system is the intersection of the structures central axis and the undisturbed water plane.

10.2.1 Hydrodynamic Forces on the Platform

The forces that are exerted on the platform as a result of the interaction with the water bodies are calculated by the HydroDyn module using the Morrison's Equation, which contains the following forces:

$$\vec{F} = \vec{F_I} + \vec{F_D} + \vec{F_B} + \vec{F_{MG}} + \vec{F_{F-B}} + \vec{F_{AM-M}} + \vec{F_{AM-MG}} + \vec{F_{AM-F}} \tag{10.10}$$

Where F_I is the inertia force, F_D the drag force, F_B the buoyancy force, F_{MG} the weight of the marine growth, F_{F-B} the force due to fluid ballasting, F_{AM-M} the added mass of the structure, F_{AM-MG} the added mass due to marine growth, and F_{AM-F} the added mass due to fluid ballasting. Marine growth on the structure is not considered in this model so the forces related to this parameter are zero; in the same way, the ballast in considered in the model as a solid part of the platform structure, therefore F_{F-B} and F_{AM-F} will also be zero.

On the other hand, the inertial loads, viscous drag and hydrodynamic added mass forces are scaled using hydrodynamic coefficients. In this case the coefficients where defined for different members of the tower, the conical section (member 1), the cylindrical section (member 2), and the spherical section at the end of the cylinder. In this case the spherical segment is modeled as a disc at the end of the cylinder (member 3). The coefficient values used in the HydroDyn module are presented in table 10.3, where C_d is the drag coefficient, C_a is the added mass coefficient and C_P the dynamic pressure coefficient; the sub indexes 1 and 2 indicate that the value is applied to the beginning or the end of the member respectively, and finally A_x indicates indicates axial components.

Member	C_{d1}	C_{d2}	C_{a1}	C_{a2}	C_{p1}	C_{p2}	A_xC_{a1}	A_xC_{a2}	A_xC_{p1}	A_xC_{p2}
1	0.80	0.80	1	1	1	1	0	0	0	0
2	0.80	0.80	1	1	1	1	1	1	0	0
3	0.80	0.80	1	1	1	1	1	1	0	0

Table 10.3: Hydrodynamic Coefficients.

10.3 Mooring System definition

Mooring systems allow floating structures to be used in deep waters where conventional jacket foundations are economically prohibitive or technically challenging. Same as the tower structure the mooring lines maintain the position and orientation of the wind turbine [5]. Although this structure provides stiffness to the tower it still allows for limited movement in all degrees of freedom, bringing new challenges to the tower and platform design. The mooring system is defined in MoorDyn [26] using three different kind of points:

- **Fixed:** For the software this nodes don't move during the simulation and are used in this case to mark the location of the mooring line anchors.
- **Connect:** These nodes are used to connect two or more mooring lines.

- **Vessel:** The movement of this nodes is defined by the movement of the tower structure, and serve as interface with the other modules.

For this model three mooring lines spaced by 120 °where used, each line connects to two out of three anchor points in the vessel as show in figure 10.4, this is done to provide stability in the yaw degree of freedom. The coordinates of each point and the chain properties are show in table 10.4 where the origin of coordinates corresponds to the center of the platform and MSL.

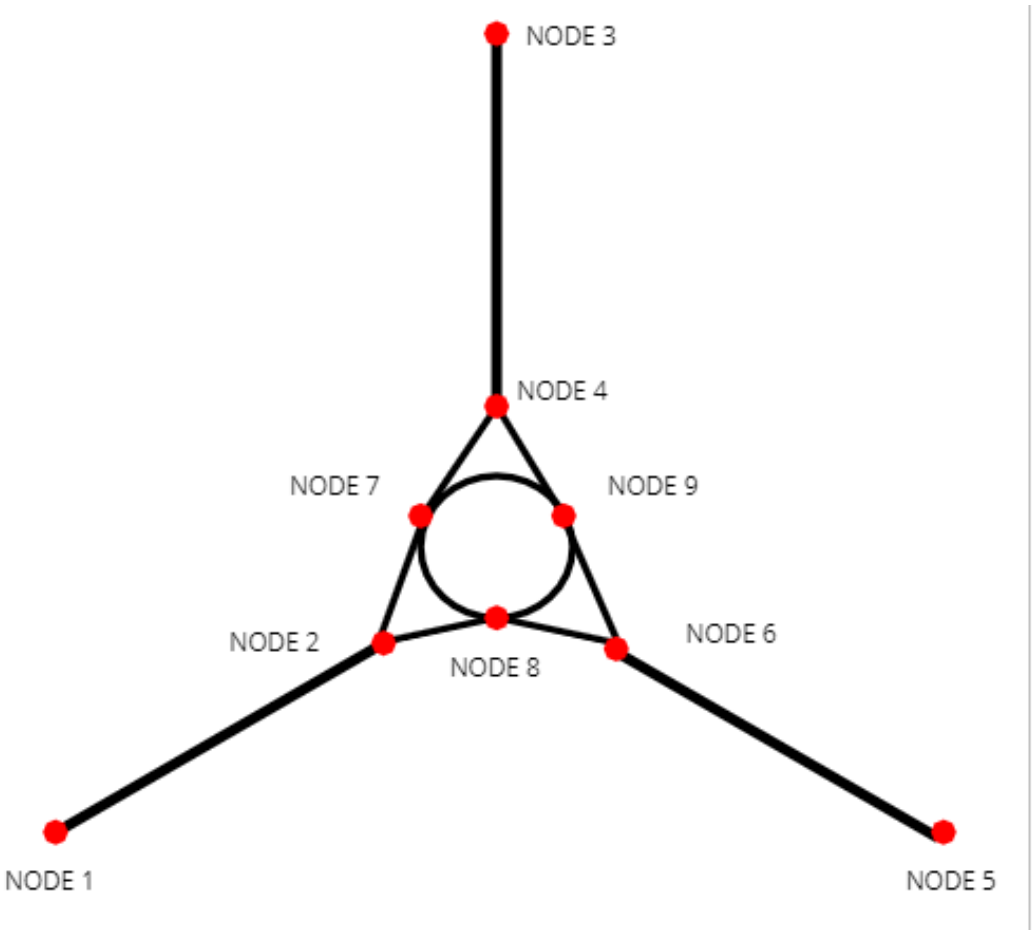

Figure 10.4: Mooring System Layout

Node	Type	X(m)	Y(m)	Z(m)
1	Fixed	-850.0	0	-250
2	Connect	-46.36	0.0	-105.66
3	Fixed	425	-736.12	-250
4	Connect	23.18	-40.15	-105.66
5	Fixed	425	736.12	-250
6	Connect	23.18	-40.15	105.66
7	Vessel	-3.90	6.76	-80.00
8	Vessel	-3.90	-6.76	-80.00
9	Vessel	7.80	0.0	-80.00

Table 10.4: Nodes used for the definition of the mooring lines in MoorDyn

Line	Connected Nodes	Length(m)	Diameter (m)	Stiffnes (KN)	Mass (Kg/m)
1	1-2	827.5	0.160	2304000	561.25
2	2-7	50	0.160	2304000	561.25
3	2-8	50	0.160	2304000	561.25
4	3-4	827.5	0.160	2304000	561.25
5	4-8	50	0.160	2304000	561.25
6	4-9	50	0.160	2304000	561.25
7	5-6	827.5	0.160	2304000	561.25
8	6-7	50	0.160	2304000	561.25
9	6-9	50	0.160	2304000	561.25

Table 10.5: Mooring Lines and Properties

10.4 Control System Definition

For the control system a version of the DTU wind controller [27] was used as a reference. Since the original controller was created for a bottom fixed wind turbine two versions of this system had to be developed for the studies performed by LIFES50+ one tuned for the Nautilus [20] and other for the OO-Star Wind Floater [30] structures, the modified parameters affect the pitch control during full load operation and are shown in table 10.6. To study the behaviour of the Windcrete tower using these control systems a step wind simulation was done for each one, considering a stepped steady wind from cut in to cut out speed and no waves . In figures 11.1 and 10.6 it can be observed that the control system developed for the nautilus is better suited for use with the Windcrete OFWT.

Parameter	Units	OO Value	Nautilus Value
Proportional gain of pitch controller	[rad/(rad/s)]	0.192201	0.208004
Integral gain of pitch controller	[rad/rad]	0.008798	0.041415
Differential gain of pitch controller	[rad/(rad/s^2)]	0.0	0.0
Proportional power error gain	[rad/W]	0.4x10^{-8}	0.4x10^{-8}
Integral power error gain	[rad/(Ws)]	0.4x10^{-8}	0.4x10^{-8}
Coefficient of linear term in aerodynamic gain scheduling, KK1	[deg]	298.32888	5.498310
Coefficient of quadratic term in aerodynamic gain scheduling, KK2	[deg^2]	693.22213	386.005941
Relative speed for double nonlinear gain	[-]	1.3	1.3

Table 10.6: Control system parameters for the Nautilus and Olav-Olsen Concepts.

The focus of the step wind simulation in the pitch comes from the fact that this degree of freedom is the more complicated to manage for these kind of turbines. The platform pitch motion of a OFWT introduces additional relative wind speed to the rotor known platform-pitch-induced (PPI) wind shear effect, which distributes

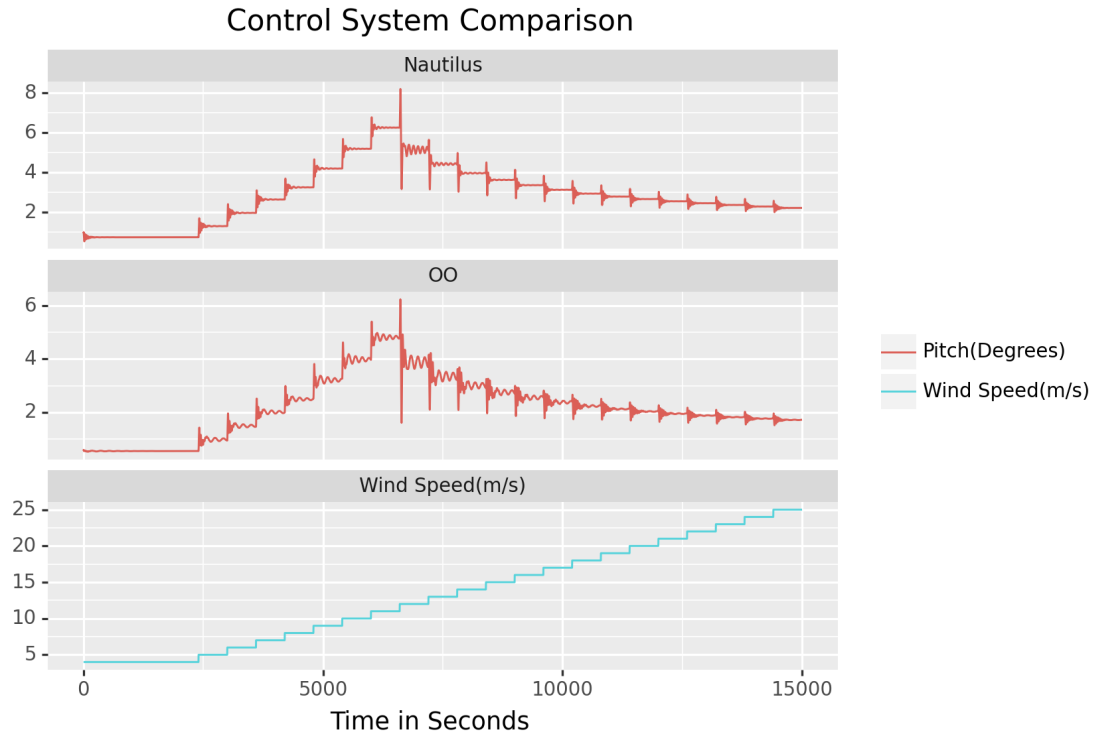

Figure 10.5: Step Wind Simulations for the Nautilus and Olav-Olsen concepts using their respective control systems.

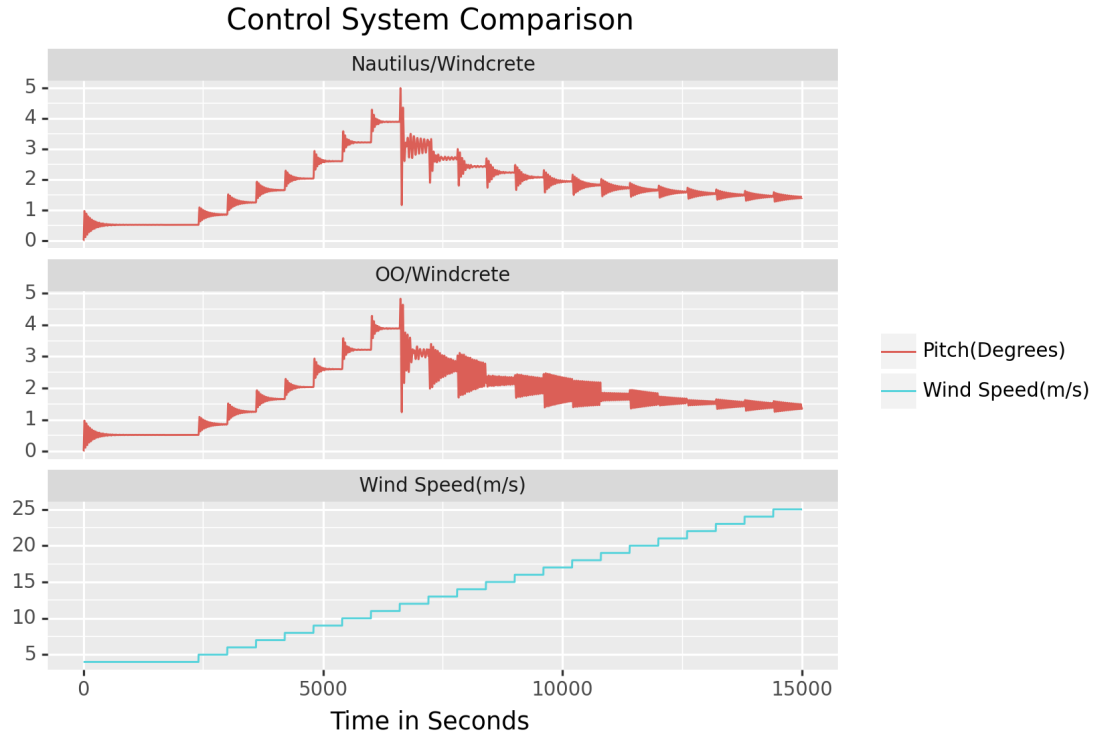

Figure 10.6: Step Wind Simulation of the Windcrete Concept using the control systems developed for the Nautilus and Olav-Olsen

linearly along the vertical axis [38]. Also, since the foundation of the turbine is less

rigid the natural frequencies of the structure are significantly lower, this leads to an unfavorable coupling between FOWT motion and the pitch control of the turbine and might produce as a result negative damping in this degree of freedom [24].

10.4.1 Tuning of the control system

During preliminary simulations of the model it was noticed that the accelerations in the nacelle where outside the permitted range for some of the design load cases, since the control system used for this simulations was not tuned specifically for the Windcrete concept it was decided that the control system parameters would be optimized for it.

For both the Nautilus and the Olav-Olsen concepts the pole-placement method [12] was used to tune the proportional-integral (PI) controller. Nevertheless other works have used differential evolution to perform optimizations on this system [29][34]. Since differential evolution is a direct search optimization method it can take into account all the specific characteristics of the tower, it was considered that this was specially convenient for a problem with so many variables as this one.

10.4.2 Differential Evolution

Differential evolution is a direct search method published in 1997 by Rainer Storn and Keneth Price [32], this means that the algorithm generates solutions a then evaluates their fitness trough a cost function that is defined for each problem.

The algorithm generates populations of vectors with different values for the variables of interest for the problem inside a previously defined range. The vectors are then recombined, evaluated and selected imitating the natural selection process, so the selected vectors that would continue on to the next generation are the better adapted for the problem environment. This process consist of four phases: initialization, mutation crossover and selection.

In the initialization phase the algorithm generates a population of Np vectors of D dimensions. Each parameter of the vector is a real number confined between an upper (L_u) and a lower limit (L_b) defined for each variable. The algorithm generates each vector using the equation 10.11 where $i = 1, 2, ..., Np-1$ and $j = 1, 2, ..., D-1$. The code uses $rand_j(0, 1)$ as a tool to generate a random number between zero and one, this will provide a uniform distribution of the vector values inside the defined range.

$$\vec{x}_{i,j} = rand_j(0, 1)(L_{ui,j} - L_{bi,j}) + L_{bi,j} \tag{10.11}$$

The vectors generated during the initialization phase are then considered objective vectors during the mutation phase. Three vectors from the population are selected, each component of a base vector (r_0) and two donor ones (r_1) and (r_2), these are combined using equation 10.12 to produce a mutant vector. The value F of the equation defines the degree in which the donor vectors will affect the base one, its value is always positive and is most cases between 0 and 1.

$$v_i = x_{r0} + F(x_{r1} - x_{r2}) \tag{10.12}$$

The objective and mutant vectors ($\vec{v}$) are then combined during the crossover phase to produce a test vector ($\vec{u}$), for this operation the algorithm employs a

crossover probability parameter (C_r) previously defined by the user with a value between zero and one. The testing vector ($\vec{u}$) is then constructed by generating a $rand_j(0,1)$ for each parameter of the vector and the comparing it with the C_r value, if the resulting value is higher than (C_r) the code will use the vector component from the objective vector, on the contrary it will use the parameter from the mutant vector.

When the population of test vectors is completed both the test and objective vector are evaluated using the user defined cost function, the objective of the algorithm is to reduce this function so if the new test vector is fitter than the objective one it will become a part of the new generations population, in this it not the case the objective vector will be used instead.

The phases of mutation, crossover and selection are then repeated until the defined number of generations is reached or the desired cost function value is achieved.

10.4.3 Definition of the parameters for the optimization

The first step for the definition of the differential evolution procedure is to determine which is the objective of the optimization, this will then shape the cost function. As mentioned before, during preliminary testing it was observed that the accelerations in the nacelle were above the permitted parameters for this variable under certain climatic conditions, these are more specifically the conditions from the design load case 1.6 using the West of Barra met-ocean conditions, therefore the optimization process will focus this value.

On the other hand, its also desirable to maintain the parts of the control system that already work, for this reason a benchmark or reference point is also needed; simulations at the beginning and end of the full load region wind speeds where used to evaluate if the new solution is also valid for moderate conditions. The tree simulation conditions are summarized in table 10.7.

Case	Wind Conditions	Hs	Tp
Benchmark Case 1	14m/s - Steady	No waves	No waves
Benchmark Case 2	19m/s - Steady	No waves	No waves
Critical Case	14m/s - ETM	15.6m	15.2s

Table 10.7: Study cases for the differential evolution optimization

The algorithm will then carry on thee three simulations for each vector of each generation, its easy to see that this method will require a considerable amount of computational power so its imperative to reduce the size of the problem as much as possible. With this in mind, only four values of the control system will be manipulated during this procedure, the range and function of this values are presented in table 10.8.

For the cost function we are interested in the following aspects of the problem:

- Reduce the accelerations in the nacelle in the identified critical case bellow $2.8m/s^2$.
- Guarantee that that the motions of the turbine are bellow the maximum values for all three cases.

Parameter	Lower Value	Higher Value
Proportional gain of pitch controller.	0	0.8
Integral gain of pitch controller.	0	0.1
Coefficient of linear term in aerodynamic gain scheduling, KK1.	0	30
Coefficient of quadratic term in aerodynamic gain scheduling, KK2.	0	700

Table 10.8: Range for the differential evolution parameter

- Guarantee that the motions of the turbine are converging to an acceptable value.
- The algorithm must be able to recognize a failed FAST simulation and discard the resulting values.

We focused the study in the pitch motions of the tower and the nacelle accelerations in the x axis, in the cost function the first peak of the pitch motion is called P_o, the last one P_e and the one with highest absolute value P. Considering these guidelines the cost function is defined by the following equations:

- For the first benchmark one:

$$Fcost_a = \begin{cases} P >= 4 & P \times 10^{10} \\ P < 4 & P \times 10^{6} \end{cases} \tag{10.13}$$

$$Fcost_b = \begin{cases} P_o >= P_e & 1 \times 10^{20} \\ P_o < P_e & 0 \end{cases} \tag{10.14}$$

- For the first benchmark case two:

$$Fcost_c = \begin{cases} P >= 3.5 & P \times 10^{10} \\ P < 3.5 & P \times 10^{6} \end{cases} \tag{10.15}$$

$$Fcost_d = \begin{cases} P_o >= P_e & 1 \times 10^{20} \\ P_o < P_e & 0 \end{cases} \tag{10.16}$$

- Critical case, where A_{na} is the absolute value of the maximum acceleration registered:

$$Fcost_d = \begin{cases} P >= 5.5 & P \times 10^{10} \\ P < 5.5 & P \times 10^{6} \end{cases} \tag{10.17}$$

$$Fcost_e = \begin{cases} P_o >= P_e & 1 \times 10^{20} \\ P_o < P_e & 0 \end{cases} \tag{10.18}$$

$$Fcost_f = \begin{cases} A_{na} > 2.8 & 1 \times 10^{20} \\ A_{na} <= 2.8 & A_{na} \times 10^7 \end{cases} \tag{10.19}$$

The final cost function can be defined as:

$$F_{cost} = \frac{Fcost_a + Fcost_c + Fcost_d}{2} + Fcost_b + Fcost_e + Fcost_f \tag{10.20}$$

The cost function is defined in this way to give priority to the reduction of the accelerations in the nacelle, this is why is A_{na} multiplied by a higher order of magnitude than the maximum values of the motions; in the same way, the sum of all the cost function elements related to the motions of the FOWT are divided by 2 to ensure that the total value is one order of magnitude bellow the cost function elements defined for the nacelle accelerations. If the FAST simulation is not completed or any of the acceleration or motion values exceeds the limits established before, the cost function will dramatically increase in value so the solution is instantly discarded.

Using this function and the parameters and ranges stated before, the simulation was carried out with ten generations with a population of 75 individuals and a value to reach of zero in the cost function.

10.5 Overall Structure Properties

The general characteristics of the structures as a whole are also significant to the tower design and are presented in table 10.9. The natural frequencies where obtained trough FAST simulations with no wind or waves and a initial perturbation in the studied degree of freedom, these are shown in figure 10.7.

Property	Unit	Value
Weight*	[Kg]	25376635.63
Center of mass in the z axis*	[m]	-92.84
Inertia*	[Kgm^2]	78277134073.28
Heave natural frequency	[Hz]	0.0308
Pitch natural frequency	[Hz]	0.0256
Roll natural frequency	[Hz]	0.0257

Table 10.9: Overall Structure Characteristics. *Values without considering the rotor nacelle assembly.

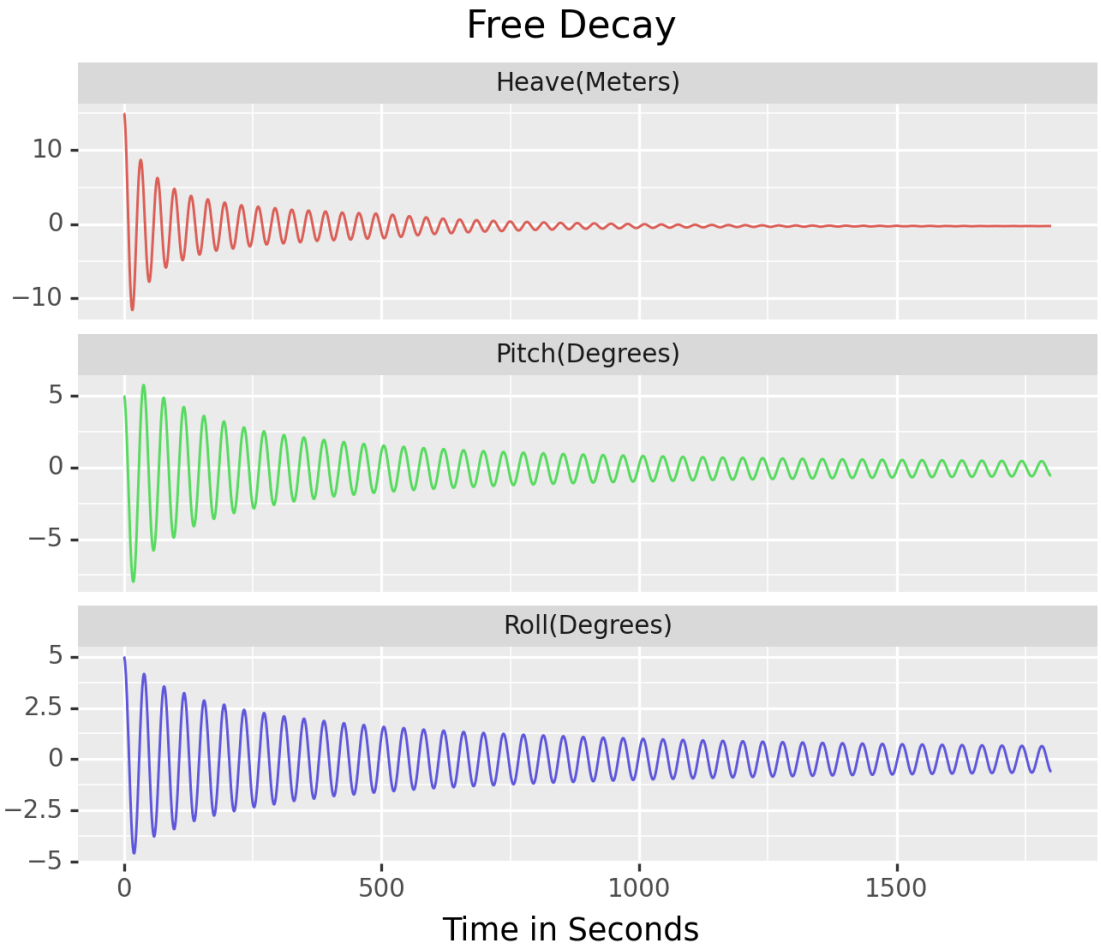

Figure 10.7: Free Decay Response

Chapter 11

Results

11.1 Control System definition

After 10 generations, the differential evolution algorithm wasn't able to reach the desired acceleration values; also the best value was reached in the third generation. Nevertheless, it was able to reduce the maximum acceleration significantly so the resulting values were used in the rest of the study, these values are presented in table 11.1. The behaviour of the Windcrete concept under the conditions used in the differential evolution algorithm with both control systems are presented in figures 11.2 and 11.1. The maximum pitch and acceleration values produced using both the Nautilus and the tuned controlled system are shown in table 11.2.

Parameter	Value
Proportional gain of pitch controller.	0.71
Integral gain of pitch controller.	0.069
Coefficient of linear term in aerodynamic gain scheduling, KK1.	27.61
Coefficient of quadratic term in aerodynamic gain scheduling, KK2.	100.336

Table 11.1: Resulting Control System Parameters

Parameter	Value with Nautilus Control	Value with Tuned Control
Pitch @ 14m/s steady wind with no waves.	2.85°	3.61°
Pitch @ 19m/s steady wind with no waves.	2.55°	2.55
Pitch @ 19m/s NTM wind with waves.	5.12°	4.9
Accx @ 14m/s steady wind with no waves.	$0.0538 m/s^2$	$0.1138 m/s^2$
Accx @ 19m/s steady wind with no waves.	$0.086 m/s^2$	$0.075 m/s^2$
Accx @ 14m/s NTM wind with waves.	$3.52 m/s^2$	$3.11 m/s^2$

Table 11.2: Maximum values for each control system

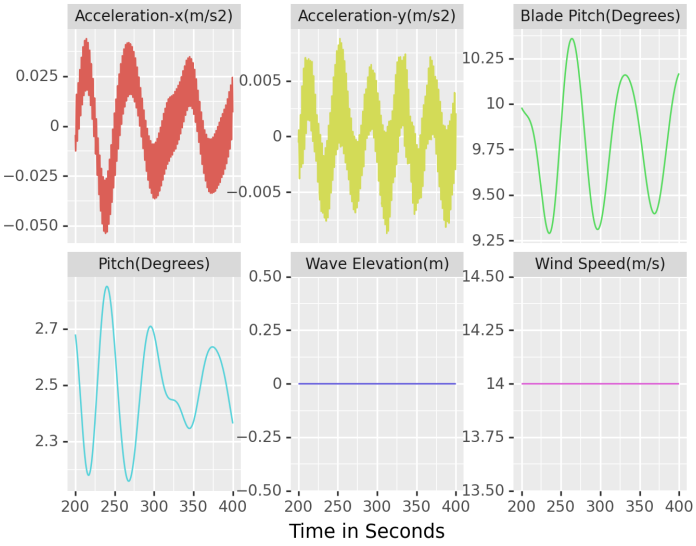

(a) 14 m/s Steady Wind and No Waves.

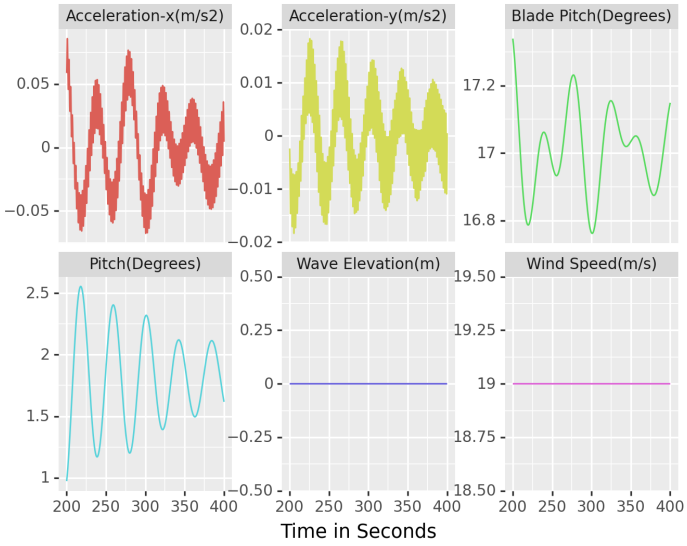

(b) 19 m/s Steady Wind and No Waves.

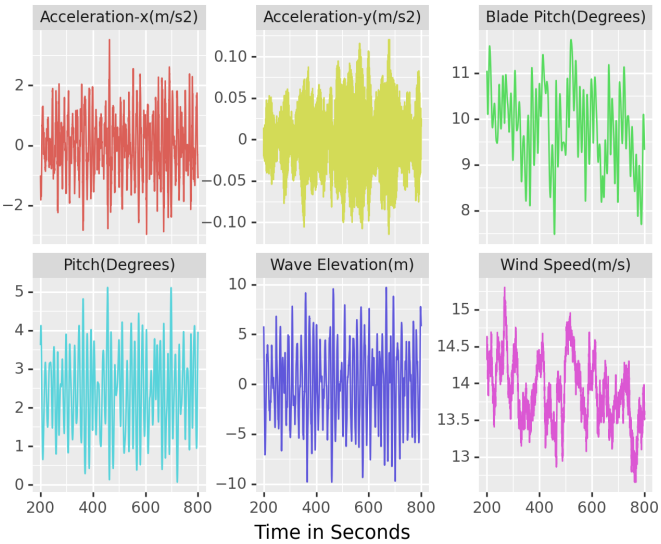

(c) 14 m/s NTM Wind, H_s=15.6m T_p=15.2s

Figure 11.1: Behaviour Under the Nautilus Control System.

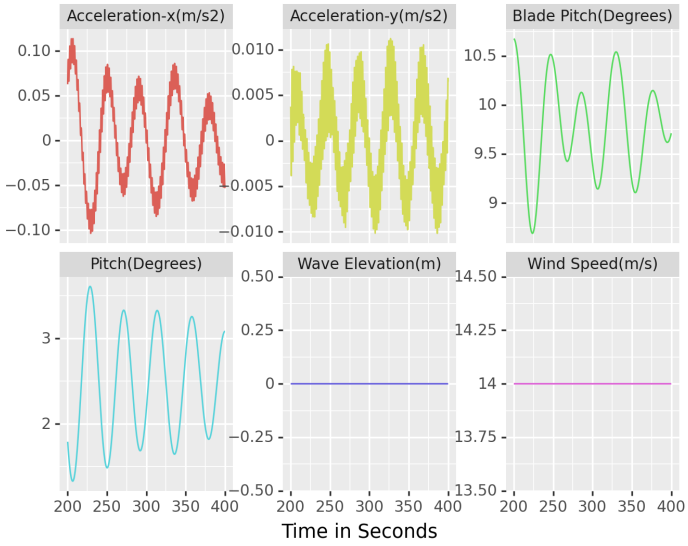

(a) 14 m/s Steady Wind and No Waves.

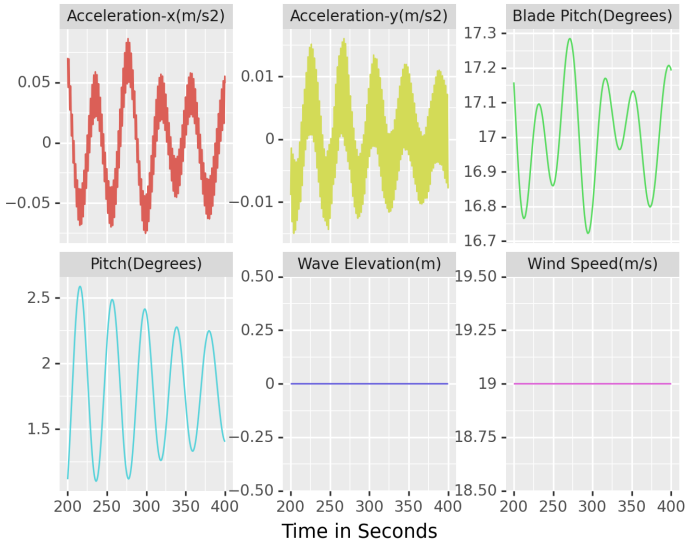

(b) 19 m/s Steady Wind and No Waves.

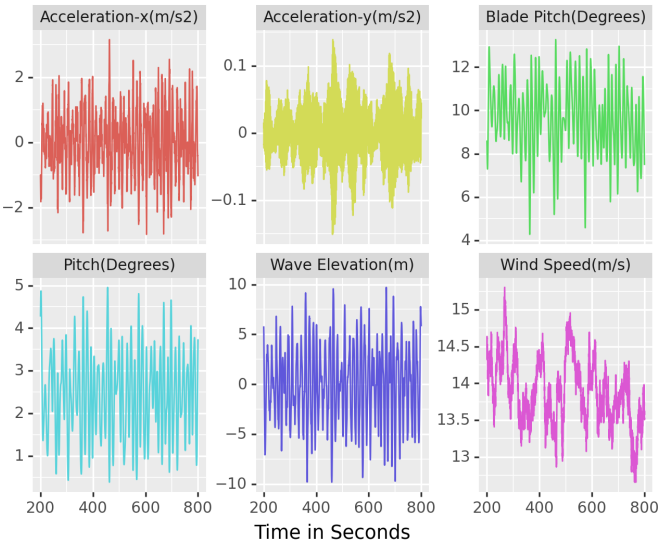

(c) 14 m/s NTM Wind, H_s=15.6m T_p=15.2s

Figure 11.2: Behaviour Under the Tuned Control System.

11.2 Motion of the FOWT Using the Site A Metocean Conditions

For each design load case, the maximum values of motion and acceleration in the nacelle reached during the simulations are presented in tables 11.3 trough 11.7. In the same way, for each DLC, the cases with higher pitch and acceleration in the nacelle are shown in greater detail in figures 11.3 trough 11.7. Only the wind speed (u) is presented in the tables, nevertheless the specific wave height and peak period can be consulted in chapter 8. All simulations are 200s longer than the time required by the IEC, this time was used to eliminate the transient behaviour of the tower at the beginning of the simulation and wont be presented in any figure.

Parameter	Conditions	Ptfm Pitch [°]	Ptfm Roll [°]	Ptfm Heave [m]	Ptfm Surge [m]	Acceleration x [m/s^2]	Acceleration y [m/s^2]	Time [s]
Ptfm Pitch	$u = 12m/s$	6.9	0.41	-0.24	11.22	-0.81	-0.01	86.7
Ptfm Roll	$u = 24m/s$	0.17	0.85	0.0397	1.41	1.03	0.0486	113.35
Ptfm Heave	$u = 24m/s$	1.75	0.44	-2.32	3.73	0.1878	0.0553	148.65
Ptfm Surge	$u = 14m/s$	6.42	0.366	-0.786	12.43	-0.733	0.0189	45.4
Acceleration x	$u = 24m/s$	4.29	-0.1474	-0.73	9.16	-3.23	-0.077	18.6
Acceleration y	$u = 24m/s$	0.71	0.50	-0.646	1.75	0.54	0.317	483.5
Avg. 10min Ptfm Pitch	$u = 12m/s$	3.59	-	-	-	-	-	-

Table 11.3: Maximum Values for the DLC 1.1 using West of Barra Conditions

Parameter	Conditions	Ptfm Pitch [°]	Ptfm Roll [°]	Ptfm Heave [m]	Ptfm Surge [m]	Acceleration x [m/s^2]	Acceleration y [m/s^2]	Time [s]
Ptfm Pitch	$u = 12m/s$	6.95	0.45	-0.0163	11.55	-1.131	0.024	89.55
Ptfm Roll	$u = 24m/s$	-0.26	0.89	-0.249	1.85	-0.2734	-0.0148	33.9
Ptfm Heave	$u = 25m/s$	1.67	0.39	-2.08	3.63	-0.301	0.123	585.375
Ptfm Surge	$u = 12m/s$	6.73	0.338	-0.9658	12.58	-0.467	0.0472	44.4
Acceleration x	$u = 24m/s$	-0.43	0.56	0.1845	-1.3525	2.845	0.0155	439
Acceleration y	$u = 24m/s$	2.47	-0.13	-0.68	4.35	0.0383	-0.3544	20.6
Avg. 10min Ptfm Pitch	$u = 12m/s$	3.6	-	-	-	-	-	-

Table 11.4: Maximum Values for the DLC 1.3 using West of Barra Conditions

Parameter	Conditions	Ptfm Pitch [°]	Ptfm Roll [°]	Ptfm Heave [m]	Ptfm Surge [m]	Acceleration x [m/s^2]	Acceleration y [m/s^2]	Time [s]
Ptfm Pitch	$u = 12m/s$	8.86	0.01	17.51	-1.27	-2.74	-0.023	32.2
Ptfm Roll	$u = 25m/s$	0.8166	0.87	-0.481	1.43	1.19	0.036	1475.6
Ptfm Heave	$u = 18m/s$	1.75	0.21	-4.52	4.40	-0.633	0.028	420.75
Ptfm Surge	$u = 12m/s$	8.86	0.013	-1.3620	17.51	-2.76	-0.031	32.3
Acceleration x	$u = 24m/s$	-2.37	0.2816	-0.87	-7.61	5.02	-0.0665	1894.5
Acceleration y	$u = 8m/s$	0.99	0.498	0.30	2.48	-0.45	0.46	100.6
Avg. 10min Ptfm Pitch	$u = 12m/s$	3.21	-	-	-	-	-	-

Table 11.5: Maximum Values for the DLC 1.6 using West of Barra Conditions

Parameter	Conditions	Ptfm Pitch [°]	Ptfm Roll [°]	Ptfm Heave [m]	Ptfm Surge [m]	Acceleration x [m/s^2]	Acceleration y [m/s^2]	Time [s]
Ptfm Pitch	$u = 12m/s$	6.1	0.916	-0.268	9.26	-0.628	-0.0311	0
Ptfm Roll	$u = 12m/s$	2.54	0.4824	-0.85	4347	-0.305	0.025	11.15
Ptfm Heave	$u = 12m/s$	-1.43	0.0945	-1.73	-2.63	-0.15	-0.0327	190.65
Ptfm Surge	$u = 12m/s$	6.1	0.916	-0.268	9.26	-0.628	-0.0311	0
Acceleration x	$u = 22m/s$	1.78	0.0347	-0.5611	4.72	-2.87	0	350.95
Acceleration y	$u = 12m/s$	-3.91	0.106	-4.1978	-0.088	0.225	-0.518	21.3
Avg. 10min Ptfm Pitch	$u = 22m/s$	0.076	-	-	-	-	-	-

Table 11.6: Maximum Values for the DLC 2.1 using West of Barra Conditions

Parameter	Conditions	Ptfm Pitch [°]	Ptfm Roll [°]	Ptfm Heave [m]	Ptfm Surge [m]	Acceleration x [m/s^2]	Acceleration y [m/s^2]	Time [s]
Ptfm Pitch	$u = 50m/s$	5.13	0.19	0.67	9.01	-0.580	-0.03	6.3
Ptfm Roll	$u = 50m/s$	0.635	1.079	-1.49	1.29	0.40	0.084	1978.6
Ptfm Heave	$u = 50m/s$	0.35	-0.406	3.96	0.56	0.25	-0.1633	204.1
Ptfm Surge	$u = 50m/s$	4.96	-0.204	-0.0508	11.82	-2.42	-0.02	231.075
Acceleration x	$u = 50m/s$	-3.27	-0.0587	-0.8825	-8.7748	4.20	-0.063	803.7
Acceleration y	$u = 50m/s$	-0.0879	0.244	0.1755	-0.364	1.346	0.427	959.1
Avg. 10min Ptfm Pitch	$u = 50m/s$	0.076	-	-	-	-	-	-

Table 11.7: Maximum Values for the DLC 6.1 using West of Barra Conditions

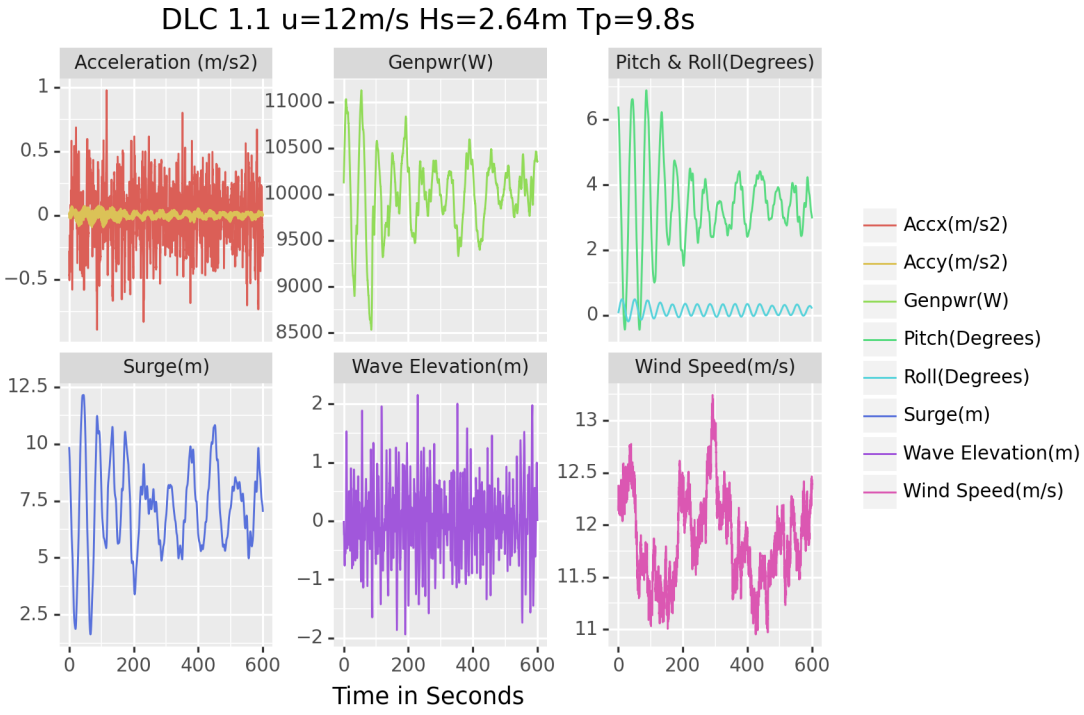

(a) Maximum Platform Pitch in the DLC 1.1

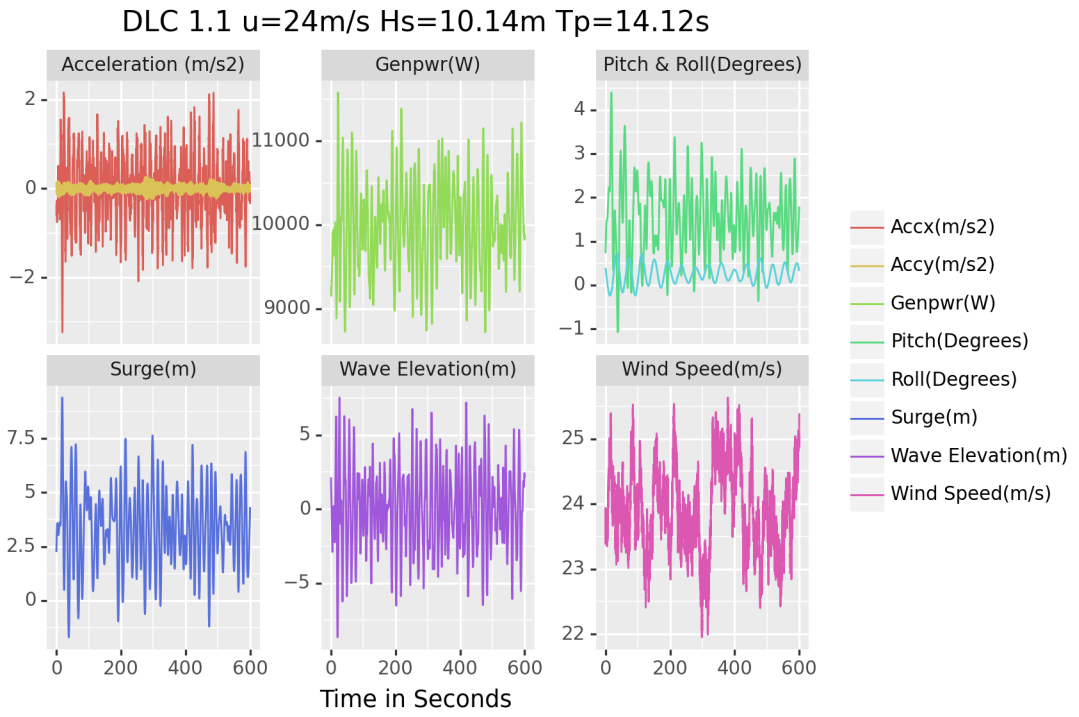

(b) Maximum Nacelle Acceleration in the DLC 1.1

Figure 11.3: FOWT Predominant motions in the DLC 1.1

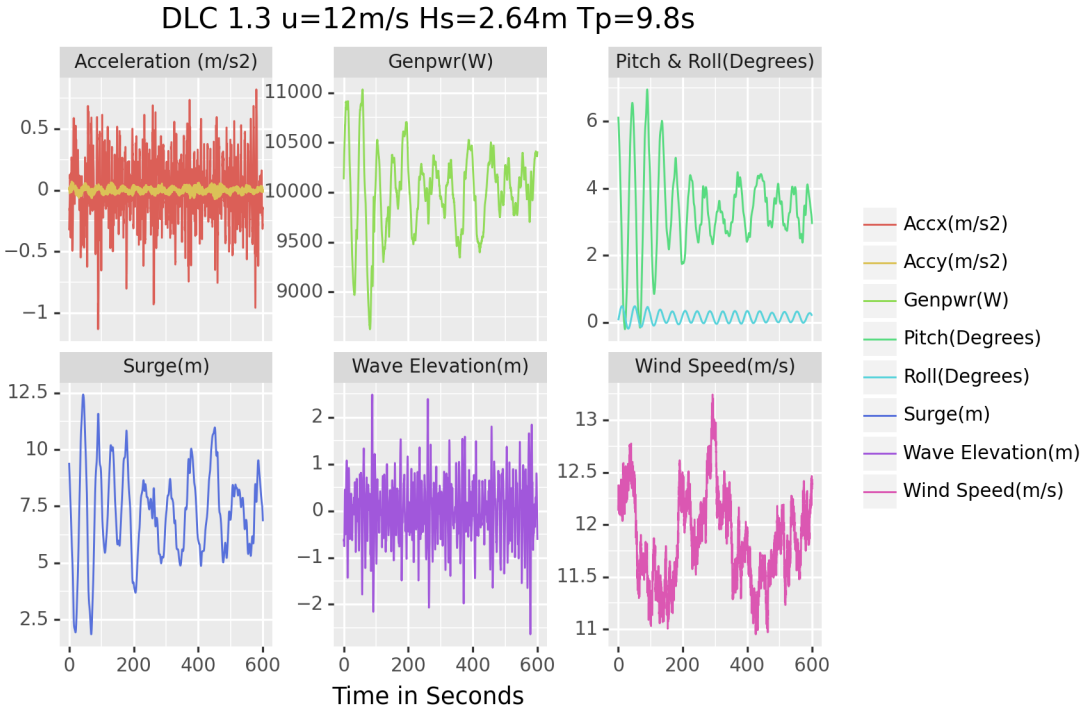

(a) Maximum Platform Pitch in the DLC 1.3

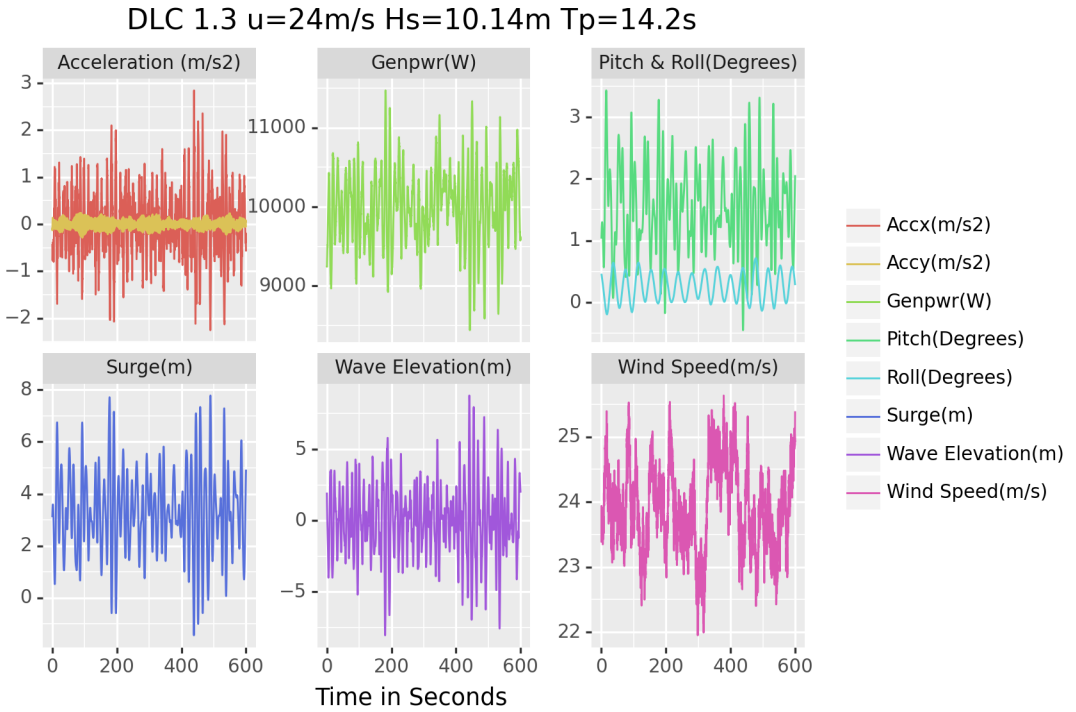

(b) Maximum Nacelle Acceleration in the DLC 1.3

Figure 11.4: FOWT Predominant motions in the DLC 1.3 using West of Barra Conditions.

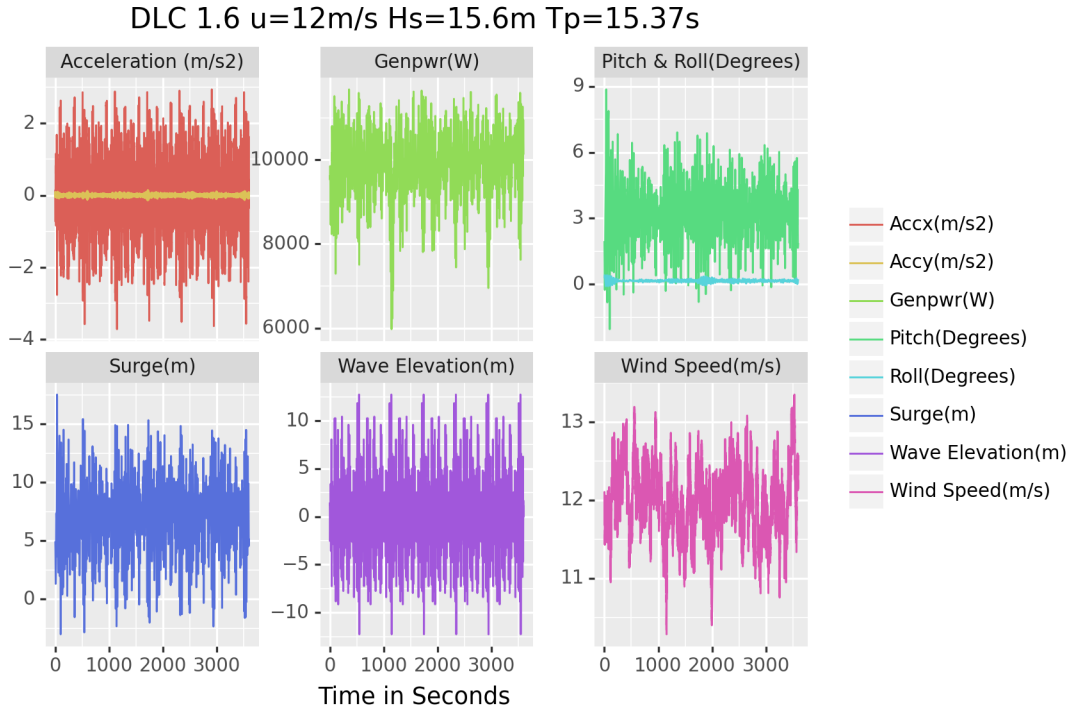

(a) Maximum Platform Pitch in the DLC 1.6

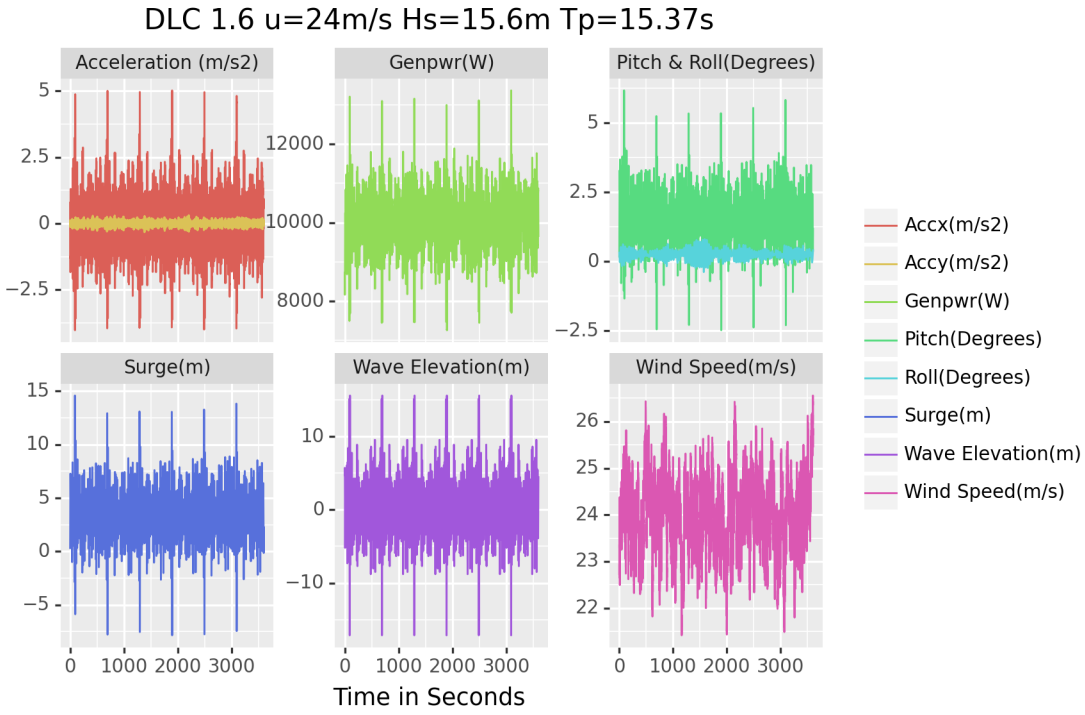

(b) Maximum Nacelle Acceleration in the DLC 1.6

Figure 11.5: FOWT Predominant motions in the DLC 1.6 using West of Barra Conditions.

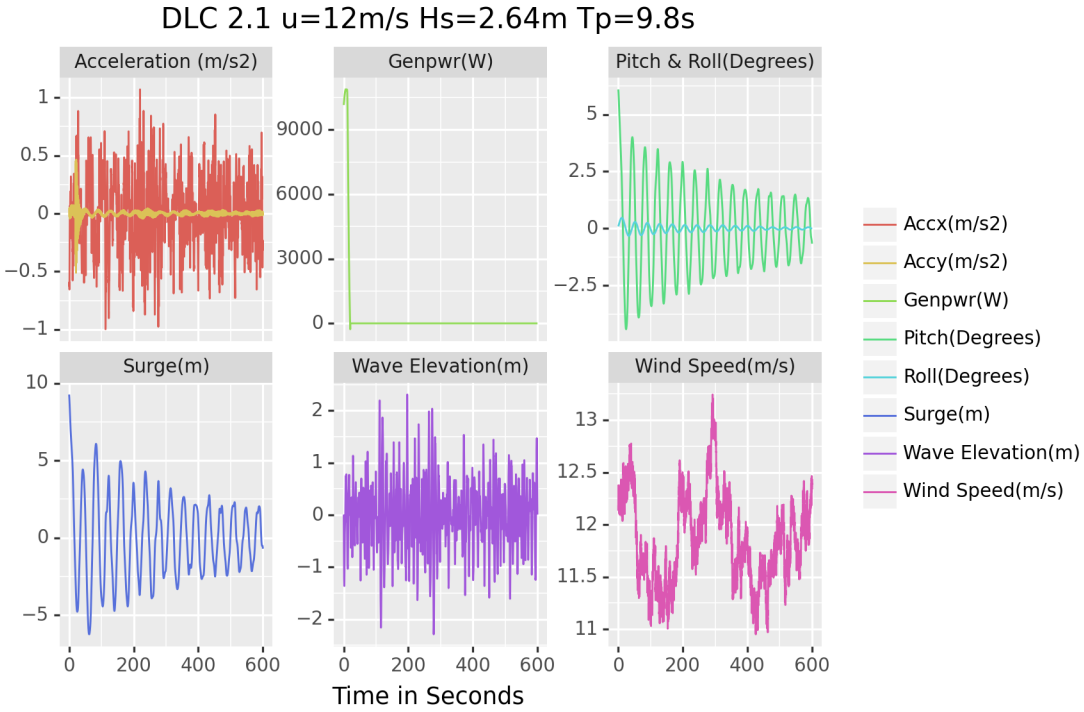

(a) Maximum Platform Pitch in the DLC 2.1

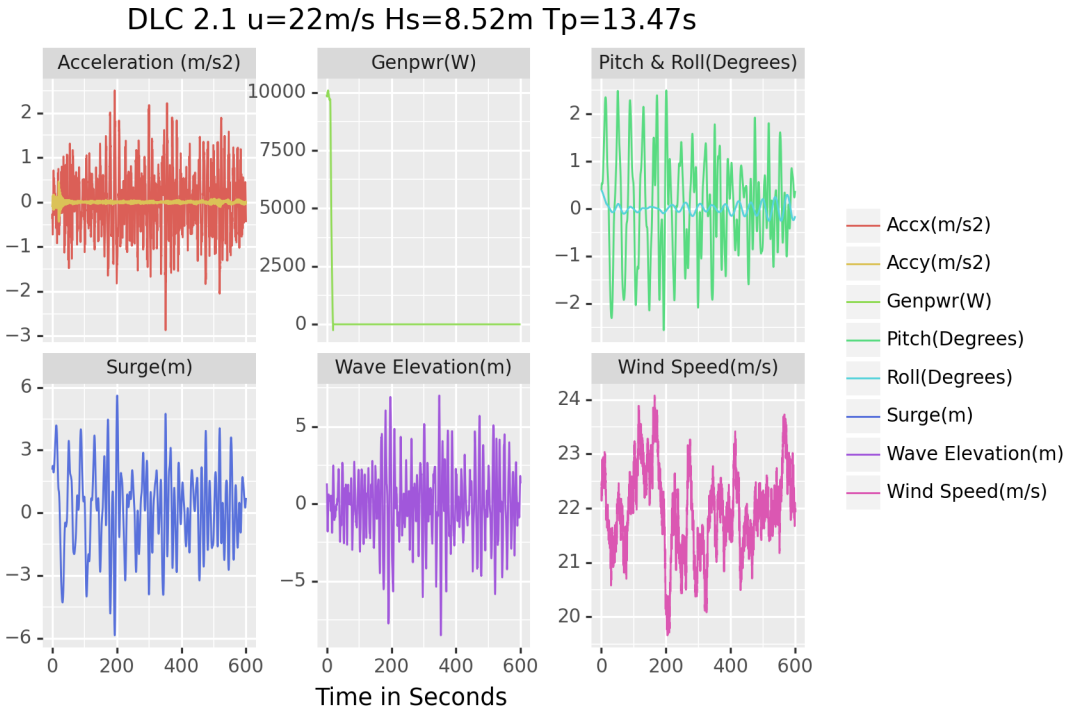

(b) Maximum Nacelle Acceleration in the DLC 2.1

Figure 11.6: FOWT Predominant motions in the DLC 2.1 using West of Barra Conditions.

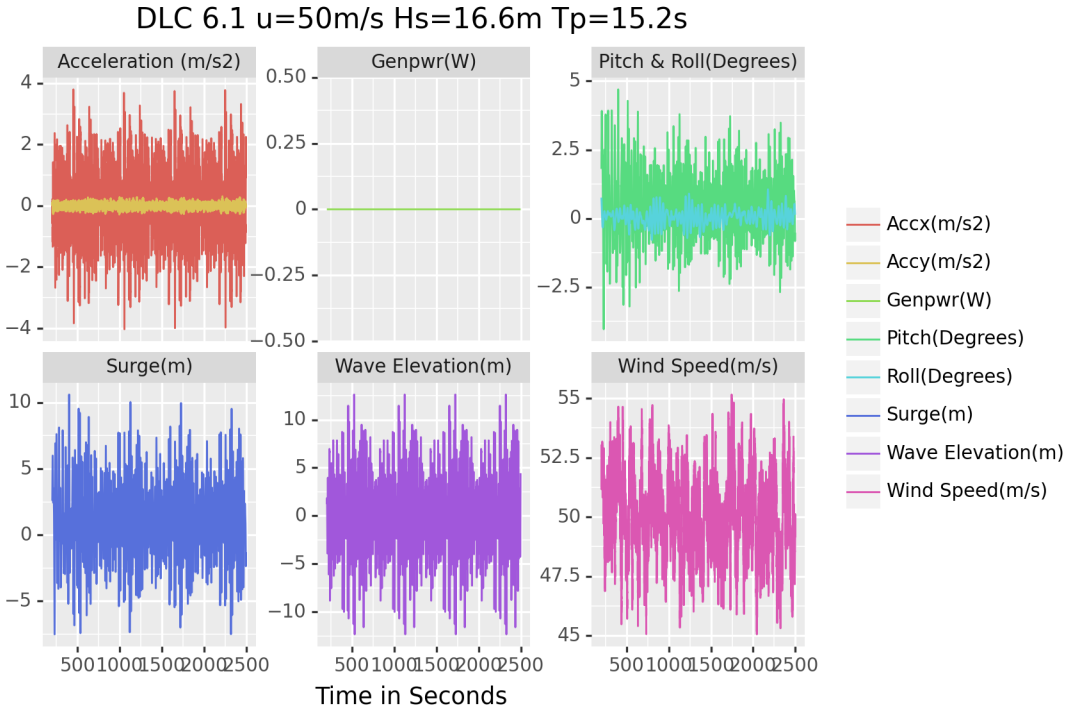

(a) Maximum Platform Pitch in the DLC 6.1

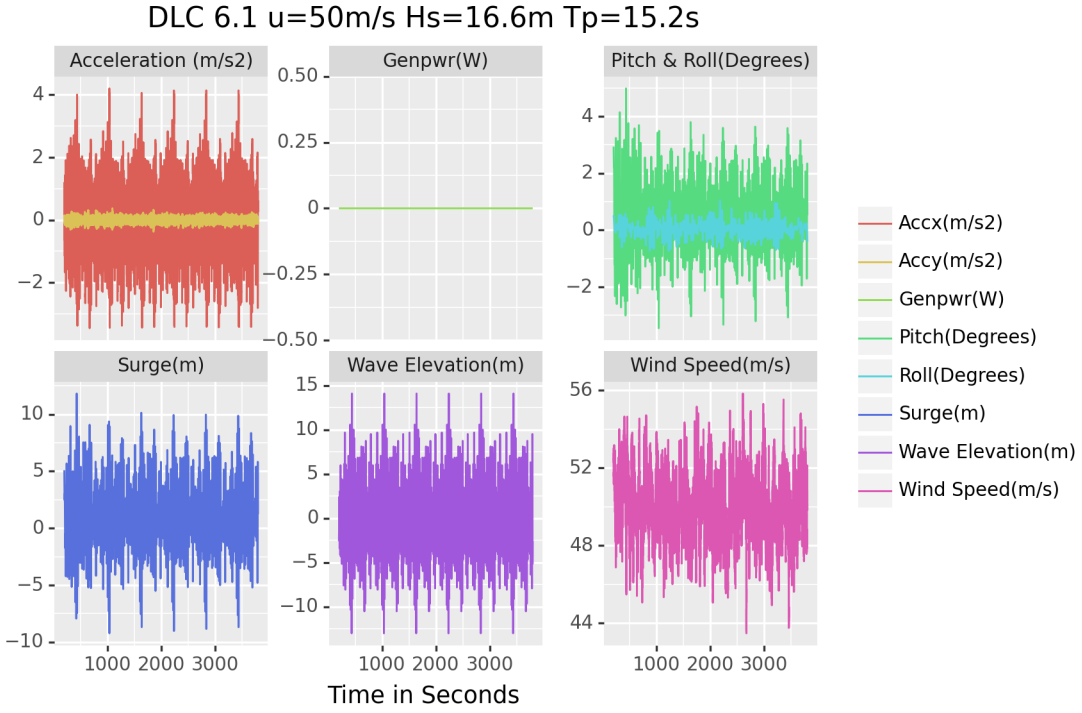

(b) Maximum Nacelle Acceleration in the DLC 6.1

Figure 11.7: FOWT Predominant motions in the DLC 6.1 using West of Barra Conditions.

11.3 Motion of the FOWT Using the Site B Metocean Conditions

For each design load case, the maximum values of motion and acceleration in the nacelle reached during the simulations are presented in tables 11.8 trough 11.12. In the same way, for each DLC, the cases with higher pitch and acceleration in the nacelle are shown in greater detail in figures 11.8 trough 11.12. Only the wind speed (u) is presented in the tables, nevertheless the specific wave height and peak period can be consulted in chapter 8. All simulations are 200s longer than the time required by the IEC, this time was used to eliminate the transient behaviour of the tower at the beginning of the simulation and wont be presented in any figure.

Parameter	Conditions	Ptfm Pitch [°]	Ptfm Roll [°]	Ptfm Heave [m]	Ptfm Surge [m]	Acceleration x [m/s^2]	Acceleration y [m/s^2]	Time [s]
Ptfm Pitch	$u = 12m/s$	4.94	0.12	-0.377	9.21	-0.44	0.023	484.7
Ptfm Roll	$u = 24m/s$	1.22	0.72	-0.157	2.56	0.0499	-0.156	478.75
Ptfm Heave	$u = 12m/s$	4.04	0.21	-1.04	10.06	0.20	0.01	170.3
Ptfm Surge	$u = 12m/s$	4.36	0.17	0.31	10.41	-0.68	0.017	445.45
Acceleration x	$u = 4m/s$	0.411	0.01	-0.388	1.14	1.13	-0.01	336
Acceleration y	$u = 24m/s$	1.084	0.405	-0.0057	2.41	0.264	0.299	282.7
Avg. 10min Ptfm Pitch	$u = 12m/s$	3.28	-	-	-	-	-	-

Table 11.8: Maximum Values for the DLC 1.1 using Gran Canaria Conditions

Parameter	Conditions	Ptfm Pitch [°]	Ptfm Roll [°]	Ptfm Heave [m]	Ptfm Surge [m]	Acceleration x [m/s^2]	Acceleration y [m/s^2]	Time [s]
Ptfm Pitch	$u = 12m/s$	5	0.095	-0.5018	9.62	-0.31	-0.001	488.35
Ptfm Roll	$u = 25m/s$	1.147	0.73	-0.12	2.42	-0.03	0.061	478.7
Ptfm Heave	$u = 12m/s$	4.13	0.198	-1.0442	10.14	-0.25	0.0046	169.55
Ptfm Surge	$u = 12m/s$	4.37	0.1731	-0.3301	10.3655	-0.19	0.018	444.9
Acceleration x	$u = 20m/s$	1.52	0.39	-0.49	3.04	-1.1103	0.086	199.55
Acceleration y	$u = 24m/s$	0.956	0.6213	-0.26	2.92	-0.0755	0.29	111.775
Avg. 10min Ptfm Pitch	$u = 12m/s$	3.29	-	-	-	-	-	-

Table 11.9: Maximum Values for the DLC 1.3 using Gran Canaria Conditions

Parameter	Conditions	Ptfm Pitch [°]	Ptfm Roll [°]	Ptfm Heave [m]	Ptfm Surge [m]	Acceleration x [m/s^2]	Acceleration y [m/s^2]	Time [s]
Ptfm Pitch	$u = 12m/s$	5.403	0.134	-0.6031	10.64	-0.63	0	1467.4
Ptfm Roll	$u = 25m/s$	1.25	0.90	-0.096	3.23	-0.2128	0.02	677.13
Ptfm Heave	$u = 12m/s$	4.50	0.	-1.47	11.51	-0.27	0.002	38.05
Ptfm Surge	$u = 12m/s$	4.72	0.13	-1.00	12.22	-1.50	0.053	39.8
Acceleration x	$u = 18m/s$	2.83	0.25	-0.49	5.82	-2.20	-0.06	3214.3
Acceleration y	$u = 25m/s$	1.51	0.46	0.023	3.02	0.421	0.456	1712
Avg. 10min Ptfm Pitch	$u = 12m/s$	3.25	-	-	-	-	-	-

Table 11.10: Maximum Values for the DLC 1.6 using Gran Canaria Conditions

Parameter	Conditions	Ptfm Pitch [°]	Ptfm Roll [°]	Ptfm Heave [m]	Ptfm Surge [m]	Acceleration x [m/s^2]	Acceleration y [m/s^2]	Time [s]
Ptfm Pitch	$u = 12m/s$	4.3	0.09	-1.062	4.95	-0.23	0.0035	44.3
Ptfm Roll	$u = 12m/s$	-0.12	0.57	-0.42	-0.089	0.069	0.10	25
Ptfm Heave	$u = 22m/s$	-1.40	-0.095	-1.73	-2.54	-0.256	-0.025	190.6
Ptfm Surge	$u = 12m/s$	6.1	0.0916	-0.268	9.265	-0.6284	-0.031	0
Acceleration x	$u = 22m/s$	1.78	0.0347	-0.561	4.727	-2.872	0	350.95
Acceleration y	-3.91	0.106	-0.088	-4.198	0.226	0.2255	-0.518	21.3
Avg. 10min Ptfm Pitch	$u = 22m/s$	0.0766	-	-	-	-	-	-

Table 11.11: Maximum Values for the DLC 2.1 using Gran Canaria Conditions

Parameter	Conditions	Ptfm Pitch [°]	Ptfm Roll [°]	Ptfm Heave [m]	Ptfm Surge [m]	Acceleration x [m/s^2]	Acceleration y [m/s^2]	Time [s]
Ptfm Pitch	$u = 41.2m/s$	3.56	-0.2264	0.023	4.82	0.012	-0.0464	3.775
Ptfm Roll	$u = 41.2m/s$	0.5235	-1.95	0.33	1.19	0.193	-0.083	2037.3
Ptfm Heave	$u = 41.2m/s$	-1.64	0.126	-1.25	-1.66	0.115	0.0264	102.45
Ptfm Surge	$u = 41.2m/s$	3.33	-0.11	-0.1645	5.4176	-0.6709	0.01	39.6
Acceleration x	$u = 41.2m/s$	1.56	-0.4847	0.53	2.90	-2.43	-0.131	280.925
Acceleration y	$u = 41.2m/s$	0.2268	1.1067	-0.1688	0.612	0.693	0.2969	2935.5
Avg. 10min Ptfm Pitch	$u = 41.2m/s$	0.309	-	-	-	-	-	-

Table 11.12: Maximum Values for the DLC 6.1 using Gran Canaria Conditions

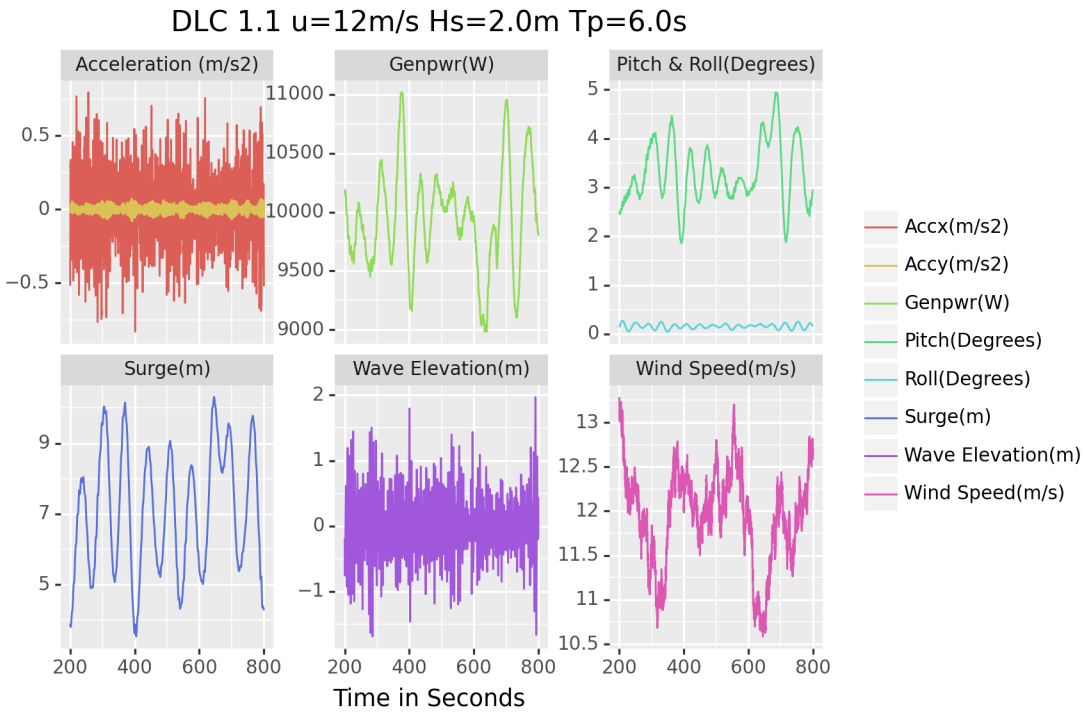

(a) Maximum Platform Pitch in the DLC 1.1

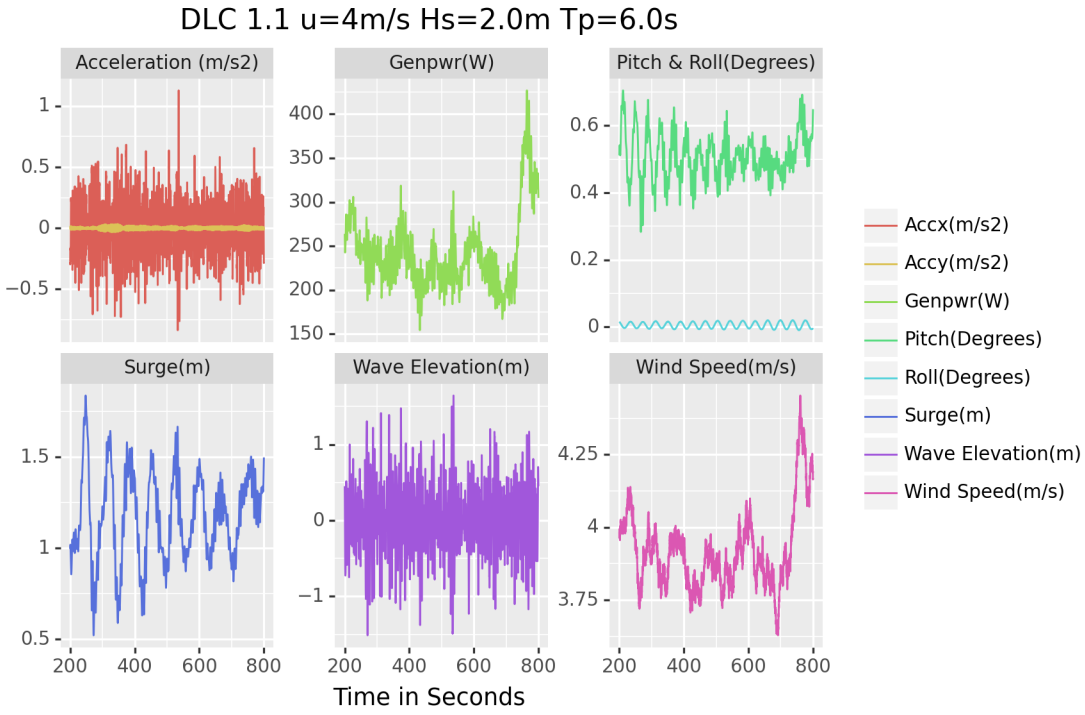

(b) Maximum Nacelle Acceleration in the DLC 1.1

Figure 11.8: FOWT Predominant motions in the DLC 1.1 using Gran Canaria Conditions.

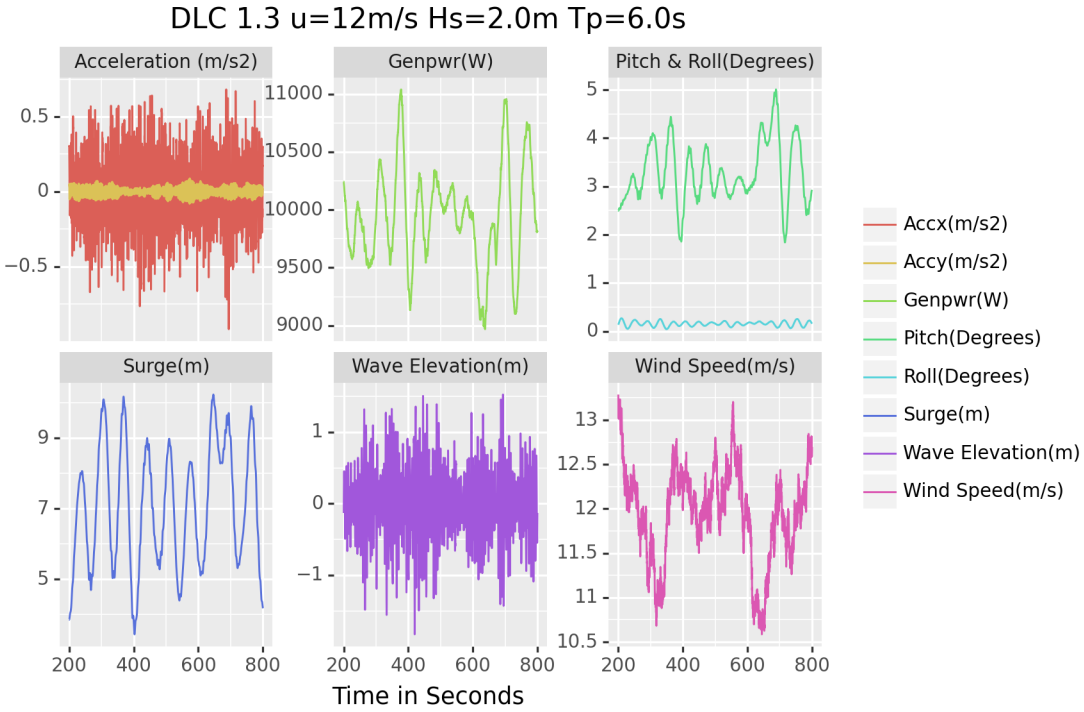

(a) Maximum Platform Pitch in the DLC 1.3

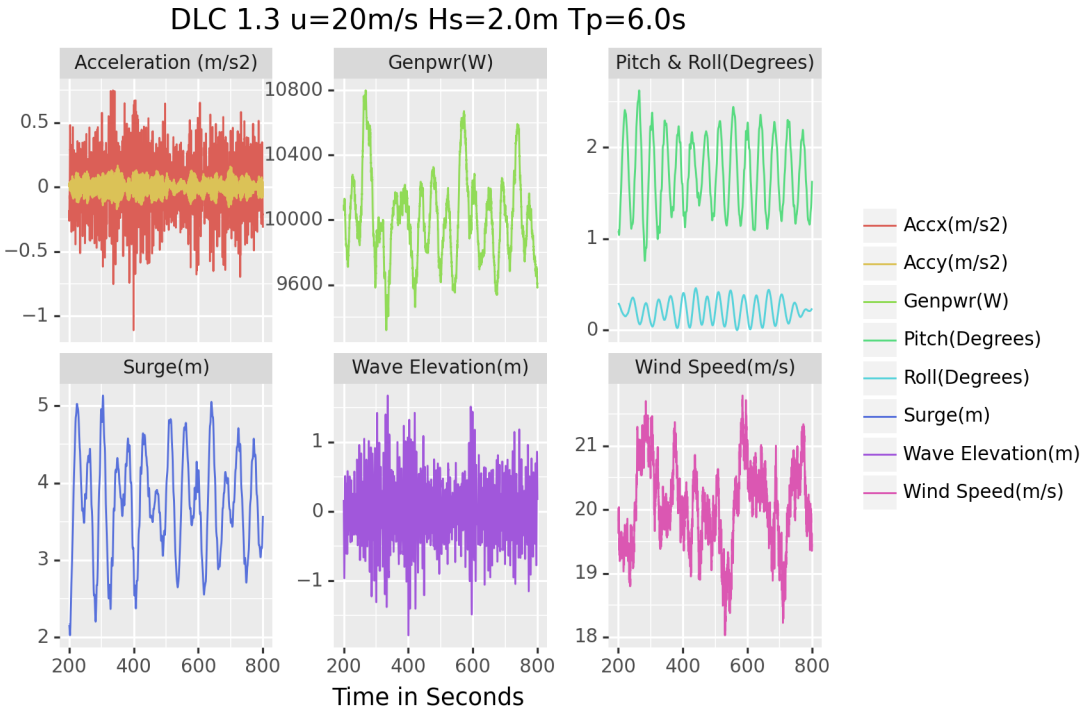

(b) Maximum Nacelle Acceleration in the DLC 1.3

Figure 11.9: FOWT Predominant motions in the DLC 1.3 using Gran Canaria Conditions.

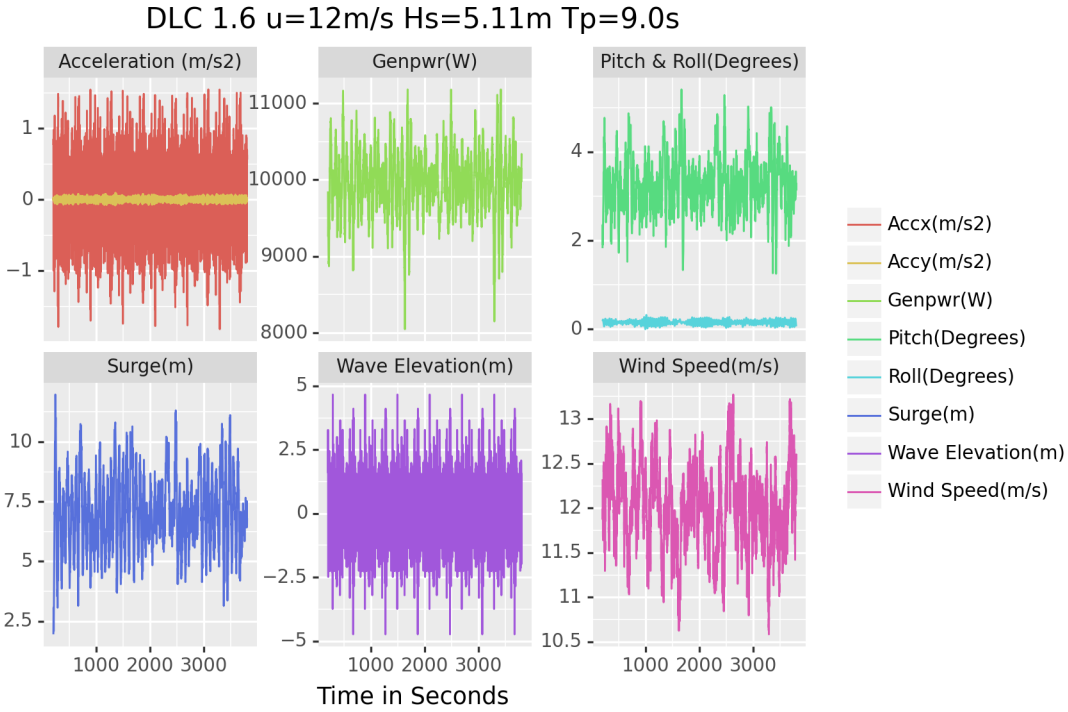

(a) Maximum Platform Pitch in the DLC 1.6

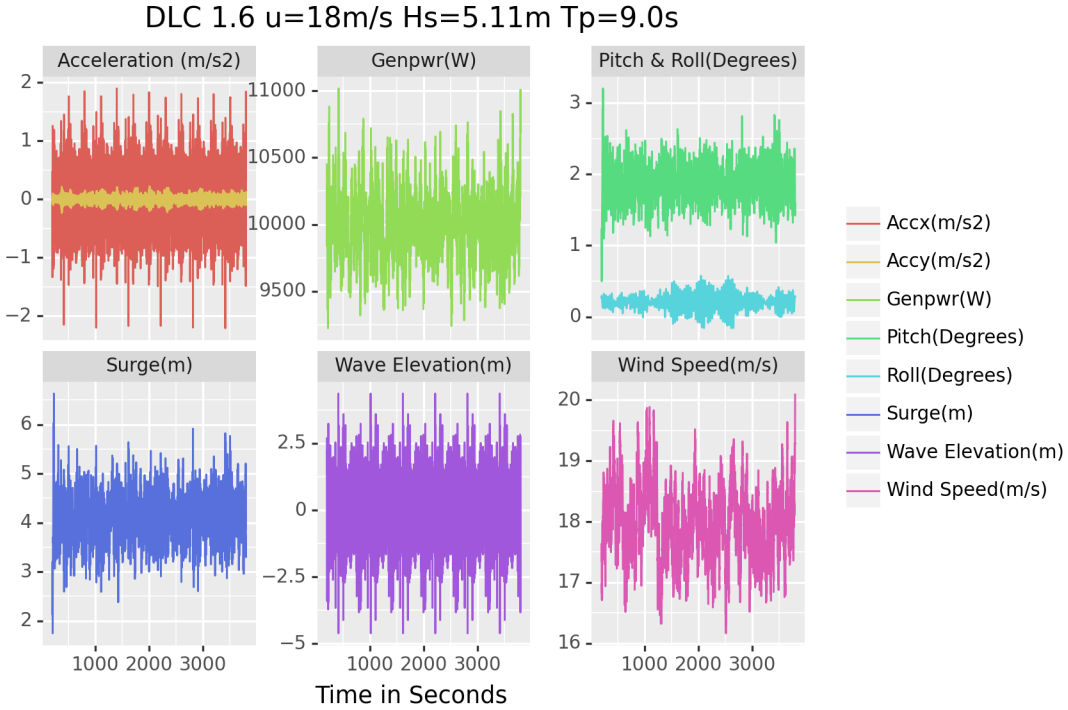

(b) Maximum Nacelle Acceleration in the DLC 1.6

Figure 11.10: FOWT Predominant motions in the DLC 1.6 using Gran Canaria Conditions.

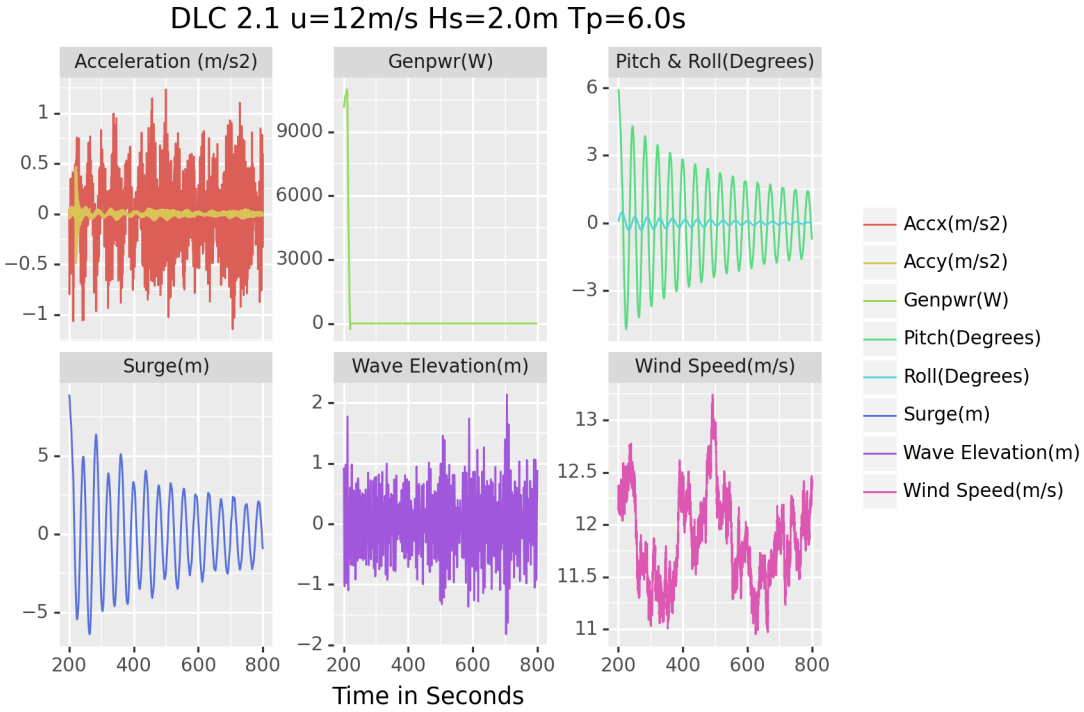

(a) Maximum Platform Pitch in the DLC 2.1

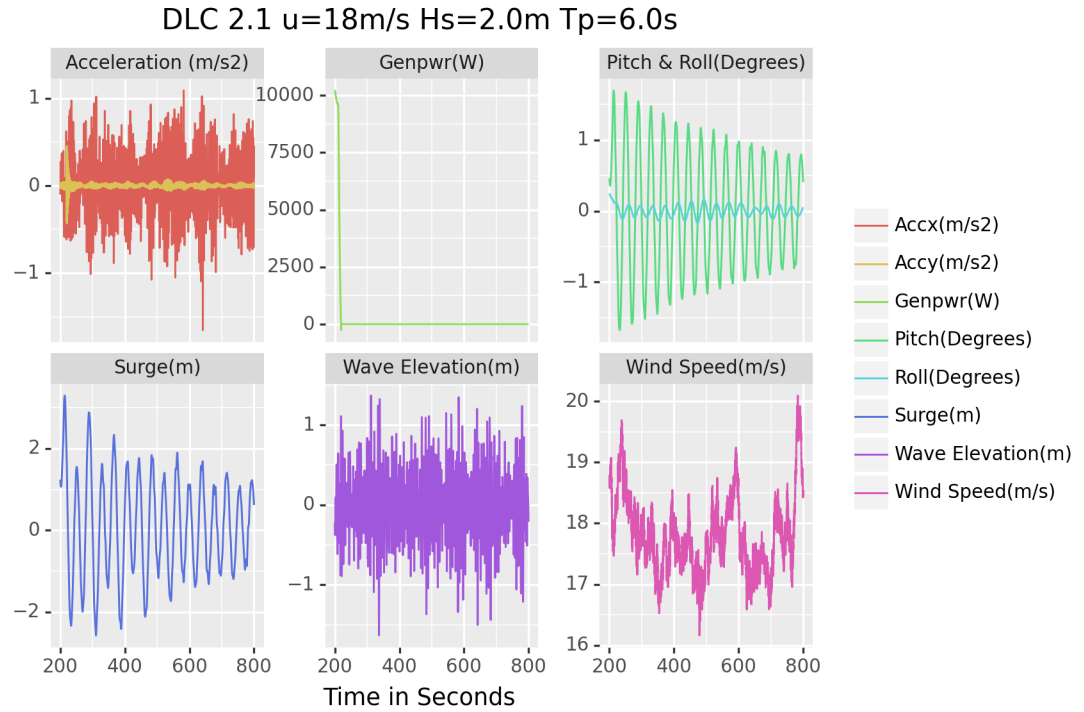

(b) Maximum Nacelle Acceleration in the DLC 2.1

Figure 11.11: FOWT Predominant motions in the DLC 2.1 using Gran Canaria Conditions.

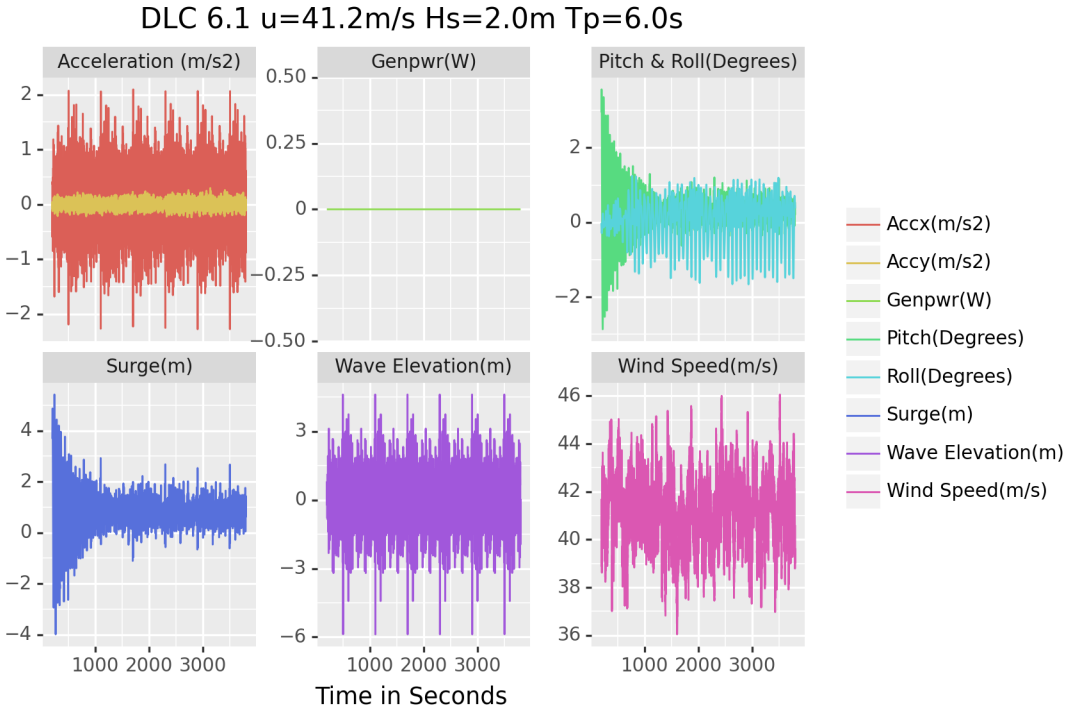

(a) Maximum Platform Pitch in the DLC 6.1

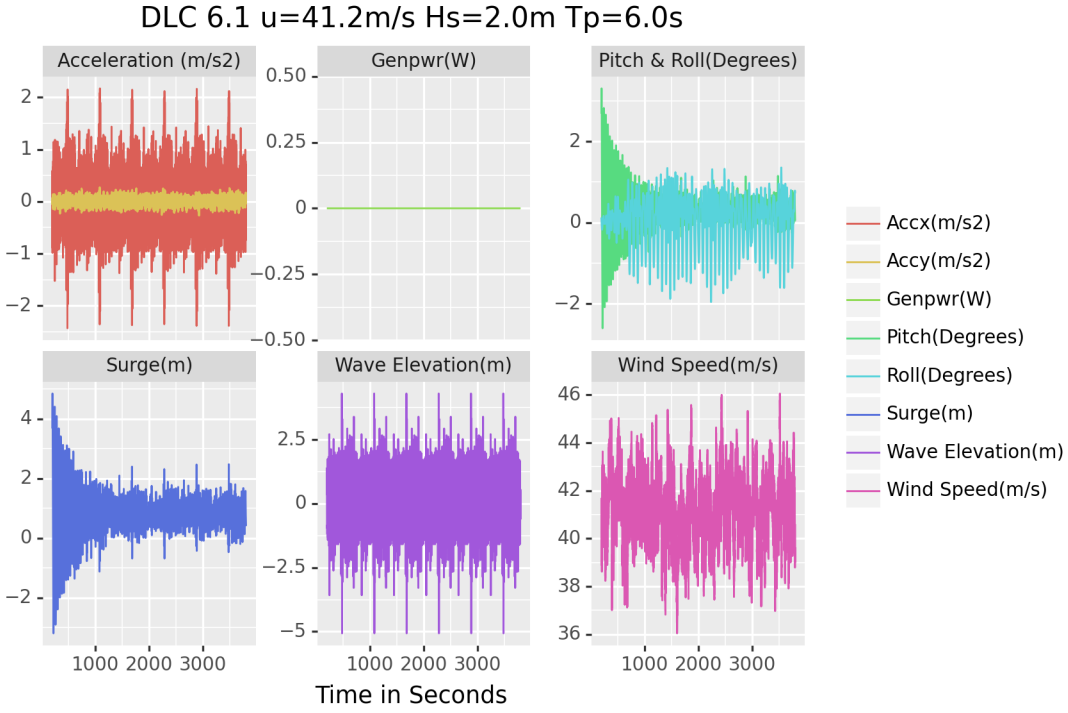

(b) Maximum Nacelle Acceleration in the DLC 6.1

Figure 11.12: FOWT Predominant motions in the DLC 6.1 using Gran Canaria Conditions.

Chapter 12

Analysis

For the control system tuning, the acceleration in the nacelle was reduced in a 13.18% while the other control values remained inside the range defined in table 4.2. While this can be considered an improvement in the tower response, the nacelle acceleration it is still above said limits ($2.8m/s^2$). On the other hand, we can see that for the case of the 14m/s wind speed and no waves the response of the structure using the tuned control system, while adequate, had higher deviations in the pitch degree of freedom. This is not a problem for the structure, but it still shows that a wide variety of climatic conditions, have to be verified while performing this method to avoid generating new issues in other sectors of the operational range.

The simulations performed in both sites showed other climatic conditions in which the structure wasn't able to perform within the established values. Without performing another simulation with said conditions ad the Nautilus control system, the influence of the tuned control system in the motion of the tower is uncertain, however, it shows that a wider evaluation of the tower behaviour before performing the optimization process could help get better results. Finally, its important to pay attention to the convergence of the method; the final value of the cost function was reached within just three generations, so certainly, performing a longer optimization process (i.e. with more generations) wouldn't really affect the final result. Therefore we could attribute the failure of the differential evolution process to one of two factors.

First we have to consider that the behaviour of the OFWT is not defined by the control system alone, many other factors like for example the position of the center of mass in relation to the center of buoyancy have a considerable effect in the stability of the structure. Therefore, it is possible that no better result could have been reached without modifying structural characteristics of the FOWT or considering a wider set of variables of the tuning system.

Secondly, since there are many factors affecting the behaviour of the tower its very likely that the solution space is a multi-modal one, meaning that it have multiple local optimum values (shown in figure 12.1). In this case, algorithm might converge to a local optimum that is not actually the most efficient solution.

Under the metocean conditions of West of Barra the maximum values of deviation in the pitch degree of freedom were surpassed in all design load cases except for the DLC 6.1, however, it can also be appreciated in tables 11.3 trough 11.7 that the peak values are reached between the first seconds of the simulation (after the first 200 seconds that were discarded); particularly in DLC 2.1 where the maximum pitch

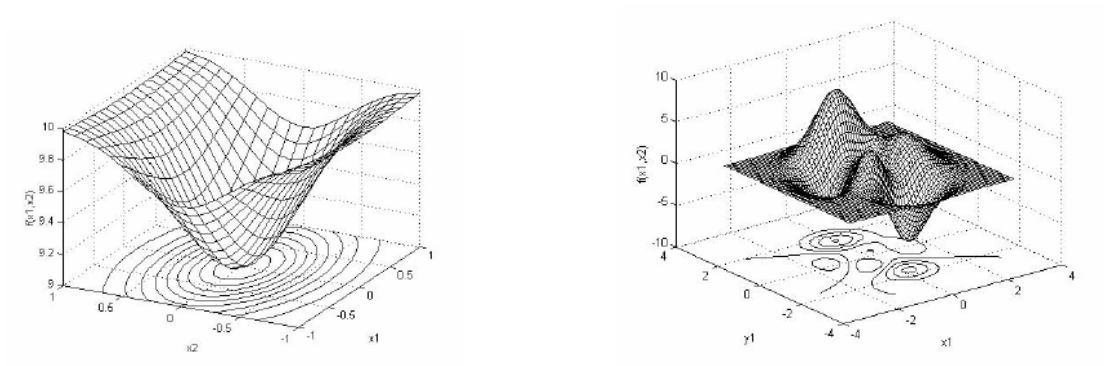

(a) Uni-Modal Objective Function (b) Multi-modal Objective Function

Figure 12.1: Objective Functions in a Differential Evolution Algorithm [32].

deviation value is reached even before the control system fault has occurred. This indicates that the time dedicated to eliminate the influence of the transient state might not have been long enough.

The case of the accelerations in the nacelle the maximum values are also surpassed in all cases, nevertheless, contrary to the pitch values, in this situation the maximum accelerations occur further into the simulation time; for the DLCs 1.6 and 6.1 a clear relation between the occurrence of the highest waves and the pitch values that exceed the established limits can be observed, discarding for this variable the influence of the OFWT initial conditions. Its important to take into account that the DLC 6.1 considering this site conditions was used to tune the control system, nonetheless, higher wave elevation values appear in the hour long simulation that where not considered in the short simulations used for the differential evolution algorithms. Indicating that the range conditions used during the differential evolution procedure was too narrow.

In the case of the simulations performed using he Gran Canaria climatic conditions, the problems produced by the transient state of the OFWT are only evident in the DLC 1.6 and 6.1 (figures 11.10 and 11.12), were a clear reduction of the values at the beginning of the simulation can be observed. In this conditions the structure was able to perform within the limits presented in table 4.2 except for the accelerations in the nacelle in DLC 2.1, where the acceleration is barely above the limit (2.5%)

Chapter 13

Conclusions

Even though the results of this simulation were not the most favorable, the insight that comes from them is very valuable and will help in future iterations of the design of the Windcrete FOWT. From this work we can observe clearly that the critical variables in the structure motion are the pitch and the nacelle acceleration in the x axis; in the same way, we were able to see how the control system is able to affect the forces that are transmitted to the FOWT structure and therefore affect its stability. Since the control system and the tower stability can be so intertwined, it is important to define a proper control system for future studies of this concept. From this study it is considered that differential evolution is still a very useful and powerful method to find the correct characteristics of a proper control system and even the tower structure; considering the experience of this work we can establish the first steps for a next iteration of the differential evolution method of this problem.

Firstly, it was clear that a better synthesis of the critical climatic conditions of the site was needed for the correct evaluation of the behaviour of the tower on the site. Nonetheless, this conditions must be evaluated while taking into consideration the increment of the computational time that this might produced.

Also, many of the problems observed in this work regarding the tower motions could be inherent to the structure definition, so it would be useful to allow the algorithm to modify some parameters of the structure in future iterations. In the same way, the method was limited by the protocols defined in the control system, for example, collective pitch blade control was used in this work since it was already defined in the control system that was used as a template, nevertheless, individual pitch blade could be a far better control strategy for FOWT [35]. On the other hand, from the results of this study it can be concluded that the 10MW Windcrete concept could operate properly under the moderate set of metocean conditions of Gran Canaria, since only the acceleration in the nacelle surpassed the allowed limits in DLC 2.1 and just by a 2.5%, also, it must be taken into account that during this DLC the turbine is suffering a control system fault that forces the turbine to stop its operation. On the contrary, for the case of the severe set of metocean conditions the tower wouldn't be able to operate within the limits established previously, furthermore, the results from DLC 6.1, were the turbine is parked, show us that independently of the control system used, the tower is not fit to operate under this conditions. Overall, this work shows how simulation softwares like FAST and testing like the one described in the 64100-3 procedures that were used for this study are a big contributor to the design process of the FOWT, pointing out problematic

features of the proposed concept and allowing developers to create and test new solutions for them.

Bibliography

[1] Carbon Trust, Floating Offshore Wind: Market and Technology Review. 2015

[2] Campos, Alexis Molins, Climent Gironella, Xavi Trubat, Pau. (2016). Spar concrete monolithic design for offshore wind turbines. Maritime Engineering. 169. 49-63. 10.1680/jmaen.2014.24.

[3] C. Bak, F. Zahle, R. Bitsche, T. Kim, A. Yde, L.C. Henriksen, A. Natarajan, M.H. Hansen. Description of the DTU 10 MW Reference Wind Turbine, DTU Wind Energy Report-I-0092, Roskilde, Denmark. 2013

[4] C. Lee and J. Newman, "WAMIT," 2016. [Online]. Available: http://www.wamit.com/.

[5] Cruz, Joao Atcheson, Mairead. Floating Offshore Wind Energy: The Next Generation of Wind Energy. 2016

[6] F. Vigara, L. Cerdán, R. Durán, S. Muñoz, M. Lynch, S. Doole, C. olins, P. Trubat, R. Guanche. D1.2Ñ Design Basis. COREWIND 2019

[7] FIB Durability of Concrete Structures in the North Sea, London, UK. 1996

[8] G.S. Bir. User's Guide to BModes. National Renewable Energy Laboratory, Golden, Colorado. 2007

[9] GWEC, Global Wind Energy Report: 2018. Global Wind Energy Council. 2019

[10] https://www.irena.org/costs/Power-Generation-Costs/Wind-Power

[11] https://www.windpowermonthly.com/article/%1523677/energy-costs-analysis-why-wind-br%oke-mainstream-2018 ,visited on 4/21/2019

[12] https://www.euractiv.com/section/energy/news/worlds-second-floating-wind-farm-sets-sail-for-portugal/

[13] IEA, Renewables 2O18: Analysis and Forecasts to 2O23, International Energy Agency, Paris (2018)

[14] IEA, World Energy Balances 2018, OECD Publishing, Paris. 2018

[15] IEC, "IEC 61400-3, Design Requirements of Offshore Wind Turbines", International Electrotechnical Commission: Geneva. 2009

[16] IRENA, Global Energy Transformation: A roadmap to 2050, International Renewable Energy Agency, Abu Dhabi. 2018

[17] IRENA, Climate Change and Renewable Energy: National policies and the role of communities, cities and regions (Report to the G20 Climate Sustainability Working Group (CSWG)), International Renewable Energy Agency, Abu Dhabi. (2019)

[18] J. Jonkman and B. Jonkman, "NWTC Information Portal (FAST v8)," 2016. [Online]. Available: https://nwtc.nrel.gov/FAST8.

[19] J.M. Jonkman "HydroDyn User's Guide and Theory Manual". National Renewable Energy Laboratory, Golden, Colorado. 2007

[20] J. Galvan, M. Sanchez-Lara, I. Mendikoa, V. Nava, F. Boscolo-Papo, C. Garrido-Mendoza and B. J., "Definition and Analysis of NAUTILUS-DTU10 MW Floating Offshore Wind Turbine at Gulf of Maine. Experiments at Sintef Ocean and PoliMi.," Tecnalia RI, Derio, Basque Country, Spain, 2018.

[21] Joselin Herbert, G. M., Iniyan, S., Sreevalsan, E., Rajapandian, S. . A review of wind energy technologies. Renewable and Sustainable Energy Reviews, 11(6), 2007

[22] Kaldellis J, Apostolou D, Kapsali M, Kondili E. Environmental and social footprint of offshore wind energy. Comparison with onshore counterpart. Renewable Energy 2016.

[23] Kåberger, Tomas. Progress of renewable electricity replacing fossil fuels. Global Energy Interconnection. 2018

[24] Larsen, Torben, Hanson, T. "A method to avoid negative damped low frequent tower vibrations for a floating, pitch controlled wind turbine". Journal of Physics: Conference Series. 2007

[25] M. Borg, M. Mirzaei and H. Bredmose, "LIFES50+ D1.2: Wind turbine models for the design" 2018.

[26] M. Hall, "MoorDyn," 2017. [Online]. Available: http://www.matthall.ca/moordyn.html.

[27] M. Hansen and L. C. Henriksen, "Basic DTU Wind Energy controller, Tech. Rep. No. E-0028,"

[28] Musial, W., Butterfield, S., Ram, B.J. Energy from Offshore Wind: Preprint. 2006

[29] Oterino, F. Zulueta, Ekaitz Ramos, Jose Calvo, Isidro Lopez-Guede, Jose. (2013). Application of Differential Evolution as method of pitch control setting in a wind turbine. Renewable Energy and Power Quality Journal. 660-666. 10.24084/repqj11.405.

[30] O. Olsen, "OO-Star Wind Floater," [Online]. Available: http://www.olavolsen.no/nb/node/149. [Accessed 09 05 2017].

[31] P. Gómez, G. Sánchez, A. Llana and G. Gonzalez, "LIFES50+ D1.1: Oceanographic and meteorological conditions for the design" 2015.

[32] Price, K. Storn, Rainer Lampinen, J. . Differential Evolution-A Practical Approach to Global Optimization. 2005

[33] Rogelj, J., D. Shindell, K. Jiang, S. Fifita, P. Forster, V. Ginzburg, C. Handa, H. Kheshgi, S. Kobayashi, E. Kriegler, L. Mundaca, R. Séférian, and M.V.Vilariño: Mitigation Pathways Compatible with 1.5°C in the Context of Sustainable Development. In: Global Warming of 1.5°C. An IPCC Special Report on the impacts of global warming of 1.5°C above pre-industrial levels and related global greenhouse gas emission pathways, in the context of strengthening the global response to the threat of climate change, sustainable development, and efforts to eradicate poverty. 2018

[34] Raza, Syed Abdur Rahim, A.H.M.. (2013). A Differential Evolution Based Adaptive Neural Network Pitch Controller for a Doubly Fed Wind Turbine Generator System. Research Journal of Applied Sciences, Engineering and Technology. 6. 4271-4280. 10.19026/rjaset.6.3544.

[35] Salic, T.; Charpentier, J.F.; Benbouzid, M.; Le Boulluec, M. Control Strategies for Floating Offshore Wind Turbine: Challenges and Trends. Electronics. 2019.

[36] United Nations Framework Convention on Climate Change. Action on Climate and SDGs. Retrieved from: https://unfccc.int/topics/action-on-climate-and-sdgs/action-on-climate-and-sdgs

[37] WangX,ZengX,LiJ,YangX,WangH.A review on recent advancements of substructures for offshore wind turbines. EnergyConversManag. 2018

[38] Wen, B., Tian, X., Zhang, Q., Dong, X., Peng, Z., Zhang, W., Wei, K. (2019). Wind shear effect induced by the platform pitch motion of a spar-type floating wind turbine. Renewable Energy, 135, 1186–1199. https://doi.org/10.1016/j.renene. 2018.

[39] Wind Europe, The European offshore wind industry: Key trends and statistics 2016. 2017